NORTHWESTERN UNIVERSITY
Department of Civil Engineering
McCormick School of Engineering and Applied Science
The Technological Institute
Evanston, Illinois 60208-3109

REPORT DOCUMENTATION PAGE

Form Approved
OMB No. 0704-0188

[illegible]

1. AGENCY USE ONLY (Leave blank)	2. REPORT DATE	3. REPORT TYPE AND DATES COVERED
		Final Report 12/89 - 11/92

4. TITLE AND SUBTITLE

Characterization of Acoustic Emission Source to Identify Fracture in Concrete (U)

5. FUNDING NUMBERS

AFOSR-90-0101

6. AUTHOR(S)

Surendra P. Shah

7. PERFORMING ORGANIZATION NAME(S) AND ADDRESS(ES)

Dept. of Civil Engineering
Northwestern University
Evanston, Illinois 60208

8. PERFORMING ORGANIZATION REPORT NUMBER

9. SPONSORING/MONITORING AGENCY NAME(S) AND ADDRESS(ES)

U.S. Air Force Office of Scientific Research
Bolling Air Force Base, D.C. 20332

10. SPONSORING/MONITORING AGENCY REPORT NUMBER

11. SUPPLEMENTARY NOTES

12a. DISTRIBUTION/AVAILABILITY STATEMENT

No limitations

12b. DISTRIBUTION CODE

13. ABSTRACT *(Maximum 200 words)*

This report describes the theoretical basis, experimental approaches, and results of research to evaluate fracture properties of concrete using quantitative acoustic emission (AE) analysis techniques. Analytical tools were developed to process AE data. These tools included improvements in P-wave arrival analysis, AE source location calculation, and multichannel deconvolution techniques. The microfracture characteristics of mortar was evaluated using a three dimensional moment tensor analysis. Microcracking was found to be primarily mixed mode and shear. A new technique for testing concrete in uniaxial tension was developed. Using this technique localization and strain-softening behavior was examined. Microcracking was found to be evenly distributed throughout the specimen until about 80% of peak load. At this point localization began and the microcracks coalesced into a single macrocrack.

14. SUBJECT TERMS

Acoustic emission, microcracking, quasi-brittle materials, damage localization.

15. NUMBER OF PAGES

79

16. PRICE CODE

17. SECURITY CLASSIFICATION OF REPORT	18. SECURITY CLASSIFICATION OF THIS PAGE	19. SECURITY CLASSIFICATION OF ABSTRACT	20. LIMITATION OF ABSTRACT
			UL

Final Technical Report
AFOSR-90-0101

April 1, 1993

Characterization of Acoustic Emission Source to Identify Fracture in Concrete

Introduction

Quantitative acoustic emission (AE) techniques have been used by a number of researchers to evaluate microstructural damage in a variety of materials. An acoustic emission is a highly localized release of strain energy in a stressed material. This strain energy propagates to the surface of the specimen where it is monitored by one or more ultrasonic transducers. AE activity results from microcracking and other irreversible changes in materials. AE analysis is analogous to seismology, the only difference being the scale of fracture. AE techniques may be considered a *passive* nondestructive testing technique.

Acoustic emission techniques are well-suited for the analysis of internal damage. Quantitative AE analysis can be used to evaluate microfracture characteristics, through an inverse analysis of the recorded waveforms. The goal of this research program was to employ quantitative AE models to problems of fracture in concrete. In the course of the program new methods of analysis were developed that can improve existing techniques. The results of the research have revealed some new conclusions on the nature of microcracking and damage evolution in cement-based materials.

Summary of Technical Accomplishments

The technical accomplishments of the research program fall under two general categories. The first deals with the tools and analysis techniques that were developed. The second category deals with the applications of these techniques to experimental investigations of damage in cement-based materials. The results of this research has been published (or submitted for publication) as listed below. Details of the experiments, the analysis techniques and the experimental results are summarized in the appendices. A brief summary of these topics follows.

Tools for Analysis

In order to fully utilize the potential of quantitative AE techniques, a number of analytic methods had to be developed. These new methods included an algorithm for determining the first P-wave arrival time, an improved source location method, and a multichannel deconvolution technique for AE waveform inversion.

Improved Source Location Technique

The location of the AE activity has importance on several levels. The first is interest in the location itself. In cement-based materials, AE events result from microcracking, grain boundary sliding, and other fracture process zone (FPZ) activities. Therefore the location of AE events is used to track the extent and evolution of the FPZ. The location of an AE source relative to the locations of the transducers is a function of the arrival time of the stress waves at the transducers, and the velocity of those waves in the material. First, a data filtering algorithm was designed to automatically determine the AE signal arrival times at the various transducers. Second, a nonlinear least-squares method was developed to estimate the AE source location from the previously determined arrival times. This method treats the three Cartesian coordinates as well as the wave velocity as unknowns. The location of the event, the wave velocity, and an error term are all evaluated from the arrival time data. In addition to a modest improvement in accuracy, the newly developed routines produced a dramatic increase in data analysis capacity.

New Deconvolution Technique

Once the location of the event is determined, elastodynamic and deconvolution techniques can be applied to the data to estimate characteristics of the source event. The basis of the quantitative AE model is that all the components of the process can be evaluated using linear system theory. Functions representing spatial and temporal properties of the source event, the resulting wave propagation, and the ultimate measurements processes can all be evaluated. These processes are all related through a series of convolutions. The properties of the source function are determined through *deconvolution* of the measured signals with the known wave propagation and measurement transfer functions. Deconvolution is in itself a fairly ill-posed problem. In this application it is further complicated by the problem of multiple deconvolutions at multiple channels. A fairly robust time-domain technique was developed to perform the deconvolution. The algorithm is based on a multi-channel iterative technique. The details are described in appendix A.

Experimental Results

The results of the experimental investigations brought out two major findings on the nature of damage in cement-based materials. The first finding has to do with the characteristics of individual microcracks, and the second deals with the evolution and interaction of microcracks during a loading cycle. As a part of the analysis, the characteristics of wave propagation in cement-based materials was examined.

Analysis of Wave Propagation in Cement-based Materials

Analytical models for evaluating wave propagation through elastic materials generally assume a homogeneous, nondispersive medium. Concrete, mortar and other cement-based materials are both inhomogeneous and discursive. In order to quantify these effects, a *point source/point receiver (PS/PR) ultrasonic technique* was used to investigate wave propagation characteristics in these materials. Cement paste, fine and coarse mortars, and concrete were all examined for their frequency dependent attenuation properties. All of the materials were found to be highly attenuative. The amount of attenuation was found to be greatest in the materials with the highest degrees of inhomogenieties. In addition, the materials with the largest inhomgenieties showed proportionately larger attenuation in the higher frequencies.

Micromechanics of Fracture

A three dimensional analysis of microcracking in mortar beam specimens was conducted using the previously described analysis techniques. Using the multichannel inversion technique, the characteristics of individual microcracks were evaluated. The details of the experiments and results are given in appendix A. The data analysis indicates that microcracking in mortar is primarily shear and mixed mode in nature. It was hypothesized that at the scale of microcracking (volumes on order of 10000 μm), the fracture surface is extremely tortuous and irregular. For a crack to propagate through such an inhomogeneous medium, a large shear component will be required.

Strain Softening and Localization

In a second series of experiments, unnotched concrete uniaxial tension specimens were tested and the AE activity was monitored. The details of the experiment and results are presented in appendix B. The emphasis here was on capturing the localization phenomenon which is associated with the strain-softening response of these quasi-brittle materials. The specimens were not notched as is common with uniaxial tension specimens of quasi-brittle materials. An innovative experimental setup was developed in order to conduct these tests. The purpose of testing unnotched specimens was to investigate damage localization as the load increases. Traditionally, investigators have hypothesized that damage (microcracking) is fairly random and distributed during the ascending part of the stress strain curve. It was previously concluded that at peak load the damage localizes to a single damage zone (macrocrack) which controls post peak (strain softening) response. The results of this investigation show that microcracking actually begins to localize *prior* to the peak load. The locations of AE events began to localize at about 80% of peak load. This localization controls the development of damage in the material.

The results of this research program have furthered the understanding of the nature of microcracking and damage growth in cement based materials. In addition, the tools developed for AE data analysis will be valuable in future applications of this innovative technique.

Publications (only refereed journal articles are listed)

1. Maji, A.K., C. Ouyang, and S.P. Shah, "Fracture Mechanisms of Quasi-Brittle Materials Based on Acoustic Emission," *Journal of Materials Research*, **Vol. 5** (1), 1990.

2. C. Ouyang, E. Landis, and S.P. Shah. "Detection of Microcracking in Concrete by Acoustic Emission", *Experimental Techniques*, May/June, 1991.

3. C. Ouyang, E. Landis, and S.P. Shah, "Damage Assessment in Concrete using Quantitative Acoustic Emission", *Journal of Engineering Mechanics*, **117**, No. 11, November, 1991.

4. E. Landis, C. Ouyang, and S.P. Shah, "Automated Determination of First P-Wave Arrival and AE Source Location", *Journal of Acoustic Emission*, **10**, No. 1, November, 1992.

5. Z. Li, S.M. Kulkarni, and S.P. Shah, "New Test Method for Obtaining Softening Response of Unnotched Concrete Specimen Under Uniaxial Tension," Accepted for publication in *Experimental Mechanics*.

6. E. Landis and S.P. Shah, "Recovery of Microcrack Parameters in Mortar Using Quantitative Acoustic Emission," Submitted for publication in the *Journal of Nondestructive Evaluation.*

7. Z. Li and S.P. Shah, "Localization of Microcracking in Concrete under Uniaxial Tension," Submitted for publication in the *ACI Materials Journal.*

Appendix A

Submitted for publication in ***The Journal of Nondestructive Evaluation***

Recovery of Microcrack Parameters in Mortar Using Quantitative Acoustic Emission

Eric N. Landis and Surendra P. Shah

NSF Center for Advanced Cement-Based Materials
Northwestern University
Evanston, Illinois, USA, 60208

Abstract

A three-dimensional quantitative acoustic emission (AE) analysis of microcracking in unreinforced mortar beams was conducted. In order to facilitate the analysis of the large amounts of data generated by an AE test, a simplified method for the inversion of AE signals was developed. By using the theoretical Green's function for an infinite space, the multichannel deconvolution normally required of AE data inversion reduces to a nonlinear curve fitting problem. Using this procedure, microcracking in a mortar specimen was evaluated using a seismic moment tensor representation. Source-time functions for the microcracks were also recovered. The locations of the AE events were calculated, and damage localization was observed. The moment tensor analysis showed the dominant mode of microfracture to be mode II, with a limited number classified as mixed mode. A microstructural mechanism for this behavior is presented.

Key Words

Acoustic Emission, Microcracking, Fracture Mechanisms

Introduction

The "quasi-brittle" nature of cement-based materials is characterized by distributed cracking and damage which results in a "fracture process zone." The fracture process zone is defined as the region around the continuous (visible) crack in which a field of small discontinuous microcracks is found [17]. Additional properties iclude grain boundary sliding and crack bridging. Since the nonlinear and strain-softening behavior of concrete can be linked to the properties of the fracture process zone, a better understanding of these properties is very important.

Many experimental and analytical techniques have been used to investigate microcracking in cement-based materials. These methods range from direct surface observations (microscopy, photoelasticity, laser interferometry), indirect methods (compliance measurements, numerical simulations), and interior measurements (radiography, dye penetration, ultrasonics). An additional technique which can be included in the last category is the monitoring of acoustic emissions.

An acoustic emission (AE) is the stress wave which results from microcracking, dislocation movements, and other irreversible changes in a stressed material. These stress waves propagate to the surface of a test specimen where they can be measured, recorded, and analyzed. Characteristics of the AE source can be deduced by the inversion of the recorded signals. Acoustic emissions are often referred to as microseismic events due to the parallels with earthquake phenomena. AE signals are most often measured with highly sensitive piezoelectric transducers. AE event rates correspond to damage growth in materials. If an array of transducers is mounted to a specimen, the location of AE activity can be determined by the differences in signal arrival times to the different transducers. A typical laboratory acoustic emission setup is shown in figure 1.

In this paper a method of quantitative AE analysis is presented which was used to characterize microcracking in small-scale mortar beam specimens. This technique yielded new insight into the nature of damage growth in cement-based materials.

Quantitative AE Analysis

Over the last 25 years AE measurements have been used extensively to study fracture problems in a variety of materials [14]. Hsu, et al [4] established a quantitative acoustic emission model by which the source characteristics could be deduced through an analysis of the propagation medium and the measurement system characteristics. These three components interact through a convolution model such that:

$$V(t) = T(t) * \{G(t) * M(t)\} \tag{1}$$

where *V(t)* is the measured voltage transient, *M(t)* is a function representing the AE source, *G(t)* is the wave propagation function (elastodynamic Green's function), and *T(t)* is the response function of the measurement system. "*" denotes a convolution integral. Using this model, the characteristics of an AE source can be determined from the measured voltage transients if the response of the measurement system, and the wave propagation characteristics of the material are known. That is, if *T(t)* and *G(t)* are known *a priori*, then the AE source function is determined from the measured voltage transients through a series of deconvolutions.

The critical features of this model are the representation of the AE source, and the wave propagation function. These features will briefly be described below. The response of the measurement system is determined by a calibration procedure. System calibration will also be described below.

Representation of AE Sources

The basis of the AE source model is an equivalence between a discontinuity and a set of body forces which produce the same dynamic displacements in the far field. Using an equivalent set of body forces to represent microcrack formation, a solution for the displacement transients at remote locations can be determined.

A dislocation such as a microcrack may be modeled as a seismic moment tensor, M_{ij}, where[1],

$$M_{ij} = C_{ijkl} b_k dA_l . \tag{2}$$

Here, $b_k dA_l$ is a discontinuity with area, dA_l, and Burgers vector, b_k. The plane of the discontinuity has a normal vector in the l-direction. C_{ijkl} is the elastic stiffness tensor.

Equilibrium requires that the moment tensor be symmetric. A discontinuity may therefore be characterized in three dimensions by six independent components. Scruby et al, (1985), presented some examples of simple source types and their corresponding moment tensor representations.

The stiffness tensor for an isotropic elastic solid may be written as [13]:

$$C_{ijkl} = \lambda \delta_{ij} \delta_{kl} + \mu \left(\delta_{ik} \delta_{jl} + \delta_{il} \delta_{jl} \right) \tag{3}$$

where λ and μ are the Lamé constants. The corresponding moment tensor representation is then:

$$M_{ij} = \left[\lambda b_k n_k \delta_{ij} + \mu \left(b_i n_j + b_j n_i \right) \right] \Delta A, \tag{4}$$

where n_j is the jth component of the unit normal vector, and ΔA is the area of the microcrack plane.

Since M_{ij} is a tensor quantity it may be rotated to any coordinate system using the laws of tensor transformation. As will be shown, microcrack parameters such as volume, slip, and orientation can be determined from the principal values and directions of the moment tensor.

Far-Field Displacements Due to an AE Source

The wave propagation due to an AE event must satisfy the differential equation of motion for the material. The solution for the far-field displacement, u_i, in an elastic medium due to a body force, f_j, acting on a volume, V, can be written as [1]:

$$u_i(\mathbf{x}, t) = \int_{-\infty}^{\infty} \int_V G_{ij}(\mathbf{x}, \xi, t - \tau) f_j(\xi, \tau) d\xi d\tau. \tag{5}$$

where $G_{ij}(\mathbf{x}, \xi, t - \tau)$ is the elastodynamic Green's function for the medium. The Green's function represents the ith displacement component at location, $\mathbf{x}$, and time, t, due to an impulsive force acting at ξ, and time, τ, in the j-direction. Using this formulation, the solution for the displacements due to any force function can be determined by the convolution with the appropriate Green's function. This type of Green's function is often referred to as a Green's function of the first kind. If the size of V is small compared to the separation between the source and receiver then the source can be assumed to be a point, and the spatial integration is removed from equation (5).

If the monopole force, f_j, in equation (5) is replaced with a dipole force function, M_{ij}, then equation (5) can be written:

$$u_i(\mathbf{x},t) = \int_{-\infty}^{\infty} G_{ij,k}(\mathbf{x},\xi,t-\tau)M_{jk}(\xi,\tau)d\tau, \tag{6}$$

where $G_{ij,k} = \partial G_{ij}/\partial \xi_k$ is referred to as a Green's function of the second kind. If equation (6) is convolved with a measurement system response function, the result is equation (1). Thus, a moment tensor representing an acoustic emission source can be calculated by a series of deconvolutions.

Rotation of Moment Tensor and Determination of Microcrack Parameters

As previously stated, characteristics of a microcrack AE source can be determined from the principal values and directions of the moment tensor. This derivation follows Ouyang et al [18], which was based in part on Enoki and Kishi [3].

The principal values of the moment tensor, M_{ij}, in equation (4) are governed by the equation:

$$\left(M_{ij} - M\delta_{ij}\right)x_j = 0, \tag{7}$$

where M is a principal value (eigenvalue), x_j is the corresponding principal direction (eigenvector), and δ_{ij} is the Kronecker delta. A solution of equation (7) exists only if the determinant vanishes, or:

$$\left|M_{ij} - M\delta_{ij}\right| = 0. \tag{8}$$

Equation (8) leads to a cubic equation which yields the following three principal values:

$$M^{(1)} = \left[(\lambda + 2\mu)b_k n_k + \mu\left(b_k b_k\right)^{1/2}\right]\Delta A \tag{9a}$$

$$M^{(2)} = \lambda b_k n_k \Delta A \tag{9b}$$

$$M^{(3)} = \left[(\lambda + 2\mu) b_k n_k - \mu (b_k b_k)^{1/2}\right] \Delta A. \tag{9c}$$

The three corresponding principal directions are:

$$x_i^{(1)} = b_i + n_i (b_k b_k)^{1/2} \tag{10a}$$

$$x_i^{(2)} = \varepsilon_{ijk} b_j n_k \tag{10b}$$

$$x_i^{(3)} = b_i - n_i (b_k b_k)^{1/2}, \tag{10c}$$

where ε_{ijk} is the permutation symbol.

These equations show the vector, $\mathbf{x}^{(2)}$ is in the direction normal to the plane defined by **b** and **n**. Equations (10a) and (10c) indicate that $\mathbf{x}^{(1)}$ is a vector on the plane defined by **b** and **n** in the direction which bisects the angle between them, and $\mathbf{x}^{(3)}$ is on the plane defined by **b** and **n**, and is normal to $\mathbf{x}^{(1)}$. These are illustrated in figure 2. The vector, **n**, is then defined by:

$$n_i = \frac{1}{2 (b_k b_k)^{1/2}} \left(x_i^{(1)} - x_i^{(3)} \right). \tag{11}$$

From the principal values of the moment tensor, the volume of the microcrack can be determined:

$$V = b_k n_k \Delta A = \frac{M^{(1)} + M^{(2)} + M^{(3)}}{3\lambda + 2\mu}. \tag{12}$$

In addition, the direction of microcrack slip may be expressed as an angle between **b** and **n**. If this angle is designated as α, then:

$$\cos\alpha = \frac{b_k n_k}{(b_k n_k)^{1/2}} = \frac{2\mu M^{(2)}}{\lambda \left(M^{(1)} - M^{(3)} \right)}. \tag{13}$$

Using this designation, an angle of α close to 0° indicates mode I (tensile) microcracking, whereas an angle of α close to 90° indicates mode II (shear) microcracking. It should be noted that the convention used for the principal values was: $M^{(1)} > M^{(2)} > M^{(3)}$.

Information about the microcracking characteristics is of great interest when evaluating damage in materials, since the overall response of the material is governed by properties at the microstructural level. Relationships may be determined between the microscopic and macroscopic mechanisms of crack growth, and inferences on the influence of damage on the bulk material response can be made.

Inversion of AE Data

The following information is required for the inversion of AE data, and the moment tensor analysis of microcracking: the location of the AE source, an appropriate elastodynamic Green's function, and the response functions for each transducer. Each of these items will briefly be discussed. A simplified method of inversion is then presented.

AE Source Location

The location of an AE source is of primary importance for investigations of damage localization, as well as the characterization of individual microcracks. The location of an AE source can be determined by the differences in longitudinal wave (*P*-wave) arrival times at the different transducers [19]. The location is estimated using the equation:

$$\Delta t_{a-b} = \frac{\left(|\mathbf{x}_a - \mathbf{x}| - |\mathbf{x}_b - \mathbf{x}|\right)}{c_l}. \qquad (14)$$

where $\mathbf{x}$ is the unknown location of the AE event, $\mathbf{x}_a$ and $\mathbf{x}_b$ are the locations of transducers a and b, respectively, c_l is the P-wave velocity in the material, and Δt_{a-b} is the difference in signal arrival times at transducers a and b. An iterative nonlinear least-squares method can be used to solve equation (14) [20]. A minimum of four transducers is required for a unique solution in three dimensions. Additional transducers will improve the solution since the effect of random measurement error is reduced.

Transducer Response Functions

The piezoelectric transducers used in AE testing convert mechanical disturbances to electrical signals which can be recorded. The transduction process is complex and will not be dealt with here except to note that the transducer output can be modeled as the convolution of the actual surface motion with an impulse response function [5]. Considerable research on transducer calibration has been conducted at the National Institute of Standards and Technology (NIST). This research has lead to an ASTM standard for the calibration of AE transducers [2]. The basic method is to subject the transducer to a known displacement or velocity function. The output of the transducer is then deconvolved with the displacement function to obtain the impulse response function. Once the impulse response function is known, the transducer output due to an arbitrary signal can be converted to a displacement function. The transducer is assumed to be sensitive only to normal displacements.

The deconvolution method used for both the calibration and the subsequent AE signal analysis is a time-domain least-squares method [15]. The discrete-time convolution of two time series may be represented as:

$$V(n) = \sum_{k=0}^{n} u(k)T(n-k), \tag{15}$$

where *V(n)* and *u(n)* are known time series representing the measured signal and the theoretical displacement function, respectively. *T(n)* is the unknown impulse response function. The least squares criterion is formulated such that the sum of the squared errors is minimized. This sum is written as:

$$E = \sum_{n=1}^{N} \left\{ V(n) - \sum_{k=0}^{n} u(k)\hat{T}(n-k) \right\}^2 . \tag{16}$$

where $\hat{T}(n)$ is an estimate of $T(n)$, and N is the number of points in the time series. The minimization criterion is that $\partial E / \partial \hat{T}(n) = 0$ for each $\hat{T}(n)$. This approach to deconvolution is analogous to a curve fitting problem where N parameters are used to fit N data points.

It should be noted that more common methods of deconvolution such as frequency division are not practical for this application. Problems of noise and finite signal length make the problem ill-posed for application of fast Fourier transforms [22].

Recovery of Moment Tensor from AE Signals

Once the measured AE signals are converted to displacement signals using the deconvolution procedures of the previous section, the moment tensor can be recovered through the deconvolution of equation (6). A major difficulty in this deconvolution is that analytical Green's functions exist only for a few simple geometric configurations. A number of inversion techniques have previously been used. These include the application of the Green's function for an infinite medium with corrections for boundary effects [21], Green's functions determined experimentally [8] and numerically [3], and adaptation of the Green's function for an infinite plate, [16]. The proposed inversion applies the Green's function solution for an infinite medium so that the deconvolution reduces to a multichannel curve fitting problem.

If a source occurring at the origin of an infinite medium is assumed, and only the P-wave component is considered, equation (6) may be written as [1]:

$$\begin{aligned} u_i &= G_{ij,k} * M_{jk} \\ &= \frac{\gamma_i \gamma_j \gamma_k}{4\pi(\lambda + 2\mu)c_l} \frac{1}{r} \frac{\partial}{\partial t}\left[M_{jk}\left(t - \frac{r}{c_l}\right)\right] \\ &+ \left[\frac{6\gamma_i\gamma_j\gamma_k - \gamma_i\delta_{jk} - \gamma_j\delta_{ik} - \gamma_k\delta_{ij}}{4\pi(\lambda + 2\mu)}\right]\frac{1}{r^2} M_{jk}\left(t - \frac{r}{c_l}\right), \end{aligned} \tag{17}$$

where γ_i is the direction cosine, and r is the length of the vector directed from the source to the receiver. Since the assumption of the far-field has already been made, the second term of equation (17) can be neglected as it decays much more rapidly with increasing r. Also, only the P-wave component needs to be considered since only the first few cycles of the signal will be used in this analysis. In the far-field, the P-wave is sufficiently separated from the other components.

To further simplify equation (17), the moment tensor is assumed to have a single source-time function. That is, all components of M_{ij} act with the same time dependency. Then, $M_{ij}(\mathbf{x},t) = M_{ij}(\mathbf{x})s(t)$, and equation (17) may be written as:

$$u_i(r,t) = \frac{\gamma_i \gamma_j \gamma_k}{4\pi(\lambda + 2\mu)c_l} \frac{1}{r} M_{jk} \dot{s}\left(t - \frac{r}{c_l}\right), \tag{18}$$

where $\dot{s}$ is the time derivative of the moment tensor source-time function. The time shift, $t - r/c_l$, can be eliminated since the difference in the time arguments of u_i and $\dot{s}$ is dependent only on the source-receiver distance, r, which is already known. Equation (18) may then be written:

$$u_i(r,t) = \frac{\gamma_i \gamma_j \gamma_k}{4\pi(\lambda + 2\mu)c_l} \frac{1}{r} M_{jk} \dot{s}(t). \tag{19}$$

Scruby, et al [21], showed that the effects of the specimen boundary can be corrected by approximating the incident P-wave as a plane wave. By considering the mode conversion at the free boundary, the normal displacement, v, at the surface can be expressed as:

$$v = u_r R_p, \tag{20}$$

where u_r is the radial displacement and R_p is a P-wave reflection coefficient such that:

$$R_p = \frac{2\kappa^2 \cos\psi\left(\kappa^2 - 2\sin^2\psi\right)}{\left(\kappa^2 - 2\sin^2\psi\right)^2 + 4\sin^2\psi\left(1 - \sin^2\psi\right)^{1/2}\left(\kappa^2 - \sin^2\psi\right)^{1/2}}, \tag{21}$$

where ψ is the angle between r and v as shown in figure 3. Noting that $u_i = \gamma_i u_r$, then equation (19) can be substituted into equation (20) to yield:

$$v(t) = \frac{1}{4\pi(\lambda + 2\mu)c_l} \frac{R_p \gamma_j \gamma_k}{r} M_{jk} \dot{s}(t). \tag{22}$$

Since the normal surface displacement sensitivity is assumed in the transducer convolution model, the only unknowns in equation (22) are the six independent moment tensor components, M_{ij}, and the corresponding source-time function, $\dot{s}(t)$. Equation (22) is valid as long as the signal contains no displacement components resulting from reflections at other specimen boundaries.

Ohtsu and Ono [19] compared the use of the infinite medium with a boundary correction to the solution of displacements on the surface of an infinite half-space. The infinite half-space is probably a better representation of seismic phenomena, however, the use of these solutions is extremely cumbersome. Ohtsu and Ono found very good agreement between the two formulations, indicating that the solution for an infinite medium with boundary corrections is an acceptable model for acoustic emission events.

The following substitutions will be made to facilitate a solution to equation (22). First, the moment tensor may be written as a vector using Voigt notation:

$$c_1 = M_{11} \qquad c_2 = M_{22} \qquad c_3 = M_{33}$$
$$c_4 = M_{23} \qquad c_5 = M_{13} \qquad c_6 = M_{12}$$

In addition, let:

$$H_1^q = R_p^q \gamma_2 \gamma_3 \qquad H_2^q = R_p^q \gamma_2 \gamma_3 \qquad H_3^q = R_p^q \gamma_2 \gamma_3$$
$$H_4^q = R_p^q \gamma_2 \gamma_3 \qquad H_5^q = R_p^q \gamma_1 \gamma_3 \qquad H_6^q = R_p^q \gamma_1 \gamma_2$$

where R_p^q is the previously defined P-wave reflection coefficient at the location of transducer q. Finally, let:

$$Q = \frac{1}{4\pi(\lambda + 2\mu)c_l}$$

Then equation (22) may be written:

$$v^q(t) = QH_j^q c_j \dot{s}(t), \tag{23}$$

where v^q is the normal surface displacement measured at transducer q. It should be noted that the quantity, Q, depends only on the elastic properties of the material, while H_p^q depends only on the geometric relationship between the source and the receiver. The AE source is represented by $c_j \dot{s}(t)$.

Since all AE signals were acquired digitally, equation (23) must be written in a discrete-time form:

$$v^q(n) = QH_j^q c_j \dot{s}(n), \tag{24}$$

where $n=t\Delta$. Δ is the sampling rate of the data acquisition system.

Once again, a least-squares error method is used to solve equation (24) for the unknown source terms, $c_j\dot{s}(t)$. The least-squares formulation of equation (24) is:

$$E^q = \sum_{n=1}^{NP} \left\{ v^q(n) - QH_j^q c_j \dot{s}(n) \right\}^2, \tag{25}$$

where E^q is the squared error for time series (channel) q, and NP is the number of points in that time series. Equation (25) needs to be minimized over at least six channels of data for an accurate estimate of the six independent moment tensor components. This is done by minimizing the squared error over all channels, E^{ALL}, where:

$$E^{ALL} = \sum_{q=1}^{NC} \left\{ 0 - E^q \right\}^2. \tag{26}$$

The requirements necessary for equation (26) to be minimized with respect to the c_j's and $\dot{s}(n)$ are:

$$\frac{\partial}{\partial c_j} \sum_{q=1}^{NC} \left\{ 0 - E^q \right\}^2 = 0. \tag{27}$$

and

$$\frac{\partial}{\partial \dot{s}(n)} \sum_{q=1}^{NC} \left\{ 0 - E^q \right\}^2 = 0. \tag{28}$$

respectively.

It should be noted that a unique solution is not obtained from this procedure. Some assumption about the source-time function is required for uniqueness. Since $s(n)$ is a nondimensional scalar function, it was assumed that the maximum value of $s(n)$ was set equal to one. This assumption was made so that the estimated moment tensor had the correct absolute magnitude.

A FORTRAN computer code was developed for the actual computations. The program first performed the time-domain deconvolutions required to obtain a displacement transient from each voltage transient. A step source-time function was assumed as a starting point for the iterative procedure described above. The Levenberg-Marquardt algorithm for nonlinear least squares minimization problems was used to evaluate equation (26). A routine published by Press, et al [20] was found to be very effective, and usually converged in five to ten iterations. The length of each signal used for analysis was one microsecond (16 data points at the 16 MHz sampling rate used). For this short time interval it was assumed that the signal contained no reflected displacement components from other boundaries, so that the solution for an infinite medium was valid. The microcrack parameters of volume, slip angle, and orientation were then calculated from the resulting moment tensor.

Application to Mortar Beam Specimen

The quantitative AE analysis routines were applied to a series of concrete beams with varying degrees of inhomogeniety. The goals of the research program were to determine microfracture mechanisms in various cement-based materials, examine damage localization phenomena, and to analyze the relationship between microscopic and macroscopic fracture mechanisms. The results for the mortar specimen are described here.

Experimental Program

The AE test setup shown schematically in figure 1 was used. Eight channels of data were acquired for each event. A single channel acted as a trigger which caused all eight channels to record simultaneously. The modular LeCroy system consisted of a model 6103 amplifier/trigger generator, a model 6128 fan out, eight model TR8837F transient recorders, and a model 8901A CAMAC to GPIB interface. The system was controlled via GPIB by a PC running LeCroy's "Waveform Catalyst" software. For each triggered event, 1K samples were recorded at each channel. The sampling rate was 16 MHz at 8 bit resolution. The transducers used were Physical Acoustics Corp. (PAC) model micro80. The AE signals were amplified at a gain of 60 dB by PAC model 1220B preamplifiers.

The geometry of the mortar test specimen is shown in figure 4. The mix proportion was 1: 2.6: 0.45, cement: sand: water, by weight, respectively. The sand had a maximum aggregate size of 2 mm diameter. The 28-day compressive strength of the mix was 35 MPa. The Lamé constants were: λ=35.1 GPa and μ=11.0 GPa. These constants were determined by measuring the *P* and *S*-wave velocities in the specimen using the following relationships:

$$c_l = \sqrt{\frac{\lambda + 2\mu}{\rho}} \quad \text{and} \quad c_t = \sqrt{\frac{\mu}{\rho}}$$

where ρ is the density and c_t is the S-wave velocity.

The beam was tested in a digitally controlled closed-loop MTS load frame. The feedback control for the test was the strain on the bottom face of the beam. The strain was measured with a 4 inch gage length extensometer. The feedback control was set such that this strain was increased at a rate of 0.5 μstrains per second. The load versus strain diagram is shown in figure 5. The entire test took 50 minutes. Since one of the research objectives was to observe localization of microcracking, no notch was introduced into the specimen.

A total of 107 AE events were recorded. A limitation of the measurement system was that after the system was triggered by an AE event, there was a three second minimum down time while the signals were recorded on the PC's hard disk. It is likely that some AE data was lost during this down time.

Transducer Calibration

Prior to the loading, the array of AE transducers was mounted on the specimen as shown in figure 4. The impulse response function of each transducer was estimated by subjecting them to a known displacement function and deconvolving this function with the transducer output. The known displacement function was calculated using a program by Hsu [6]. The program computes the displacement functions for a step source on an infinite plate. The step source function was approximated using a 0.3 mm pencil lead fracture on the opposite side of the specimen as the transducer. These pencil lead fractures of two different force magnitudes were performed at two different locations on the specimen for a total of four different source functions at each transducer. The corresponding displacement functions were computed, and the results deconvolved with the output signals to yield a series of four impulse resnonse functions The four different signals agreed well enough to assume that the transducer output was approximately proportional to displacement for the first microsecond. The four response functions for each transducer were averaged for use in the AE data inversion.

Verification of Inversion Technique

In order to verify the inversion procedure an independent check was made for an event where all eight channels showed clear signals. For this event the AE data from six of the eight channels was used to estimate the location, moment tensor, and source-time function for the AE source. Using this information the "forward" problem was carried out at the two remaining transducers. That is, equation (22) was used to determine the normal surface displacement functions at the two redundant transducers based on the recovered location, moment tensor and source-time function. These displacement functions were then convolved with the appropriate response functions to estimate the transducer outputs for this event. The computed outputs are compared with the actual measured outputs in figure 6. These results show a sufficiently good agreement so that it may be concluded that the model can predict far-field displacement (and transducer outputs) for a given AE source in mortar.

Experimental Results

As stated above, 107 AE events were recorded for the mortar beam specimen. Of these 96 had at least four signals of sufficient amplitude required to estimate a source location in three dimensions. Eight of the 96 however, failed to converge and could not be resolved. Therefore 88 events (82%) were located as shown in figure 7. The events were located as described above using differences in arrival times at different transducers. The arrival times were determined by a computer algorithm developed by Landis, et al [9]. It was estimated the source locations were accurate to within 2-3 mm. This estimate was based on a location calculation of an artificial source on the surface of the specimen.

As can be seen in the figure, before peak load there appears to be three areas of microcrack concentration: one very close to the centerline, and one at about 4 cm on each side of the centerline. After the peak load most events occur around the centerline of the specimen. The visible surface cracks are also shown on the figure. It seems likely that the three concentrations of prepeak events are due to very small shrinkage cracks at those locations. Li, et al [11] found random microcracking up to about 80% of peak load. At this point microcracking localized to a single crack location. It is therefore likely that these small shrinkage cracks served as a starting point for further crack growth, and that it was therefore not possible to observe true localization. Regardless of how cracks were initiated, it can be seen in the figure that they tend to start at the corners of the beam cross section. In addition, the AE events tend to occur farther up at the specimen surfaces than inside the specimen indicating that cracks have a nonuniform cross section as shown in the figure. This phenomenon was previously examined using dye penetration techniques[23].

Of the 88 events that were located, only 30 had strong enough signals at the minimum six channels required for moment tensor analysis. Since mortar is a highly attenuative material, measurement of all AE activity is difficult if not impossible. Of these 30 events four failed to converge in a reasonable number of iterations, so a total of 26 events (24% of all recorded events) were completely characterized by the moment tensor analysis.

Several recovered source-time functions are shown in figure 8. Typical characteristics of these functions are 0.4 to 0.7 μs rise time followed by a slight drop.

The unit maximum amplitude that was assumed in the inversion procedure is also illustrated.

A histogram of the recovered microcrack volumes is shown in figure 9. A majority were less than 10,000 μm^3 with a few as large as 125,000 μm^3. A histogram of the recovered slip angles is shown in figure 10. It was defined previously that the slip angle, α, is the angle between the crack plane normal vector and the direction of crack opening (Burgers vector). For purposes of classification, the microfracture mode may be defined in terms of the slip angle, α, as follows: $\alpha < 83°$ is mixed mode, whereas $\alpha > 83°$ is mode II. All of the recovered slip angles are between 75 and 93 degrees, indicating a predominance of mode II (shear) microcracking, with some mixed mode.

Discussion

The crack plane orientations are plotted in figure 11. The orientations of the microcrack planes seem to support the notion that microcracking in mortar is primarily mode II in nature. All of the microcracks shown in figure 11 are inclined with respect to the direction of principle tensile stress. Traditionally, the fracture of concrete and mortar was considered a function of its tensile strength. A mechanism is presented here which would show microscopic shear and mixed mode cracking regardless of whether the macroscopic behavior is mode I, mixed mode, or mode II.

As long as the calibration of the transducers can assumed to be absolute, that is, the transducers are actually sensitive to the absolute displacements to which they are subjected, then the volume of the microcrack is calculated using equation (12). As previously stated typical recovered microcrack volumes were in the range of 10000 μm^3. A shear crack of this volume could have an opening on the order of only a few microns [7]. At this scale the structure of the cement matrix is very irregular, and somewhat amorphous [10], as shown in figure 12. The microcrack shown in figure 12 follows an extremely tortuous path through the microstructure. If the microcracks develop in a microstructural medium as schematically shown in figure 13, then it seems likely that mixed mode and mode II could be the exclusive fracture modes. The interfacial zone between the cement paste and aggregate could also be characterized by these features.

An additional insight is illustrated in figure 14. This figure shows the recovered slip angles at each AE event, and the corresponding load at which the events occurred. It can be seen here that during initial (prepeak) damage, the microfracture tends to be more mixed mode. The post peak microfracture tends to be almost pure mode II, with the exception of the microcracking around event number 50. The microfracture is again characterized by mixed mode behavior, but here there is also a much more dramatic decrase in load, indicating rapid damage growth. A conclusion which may be made from these observations is that initial damage is characterized by fracture between cement particles, and the cement - aggregate interface. Whereas steady-state damage growth could be charcterized by friction along the crack surfaces.

It should be noted that there is another possible explanation for the dominance of shear microcracking. It is possible that there could have been some kind of systematic elimination of mode I microcracks. As was mentioned above, only 24% of all recorded AE events could be used in the moment tensor analysis due to insufficient signal amplitude at less than the minimum of six transducers. A possibility exists that either the geometry of the transducer array was biased against mode I events, or that any mode I events that did exist were not large enough in energy. Some numerical experiments were carried out to test for any bias. Mode I microcracks of a variety of orientations and locations were assumed and substituted into equation (22). The volumes of these assumed microcracks were in the range of those actually measured. The resulting surface displacements at the transducer locations were calculated. These displacements were of the same order of magnitude as those measured, indicating that there was not any bias in the transducer array geometry. The only other possibility for systematic elimination of mode I events would be if they tend to be smaller in amplitude than the mode II events.

All of this discussion about AE recovery of microcracking assumes that the moment tensor model adequately represents the physical phenomenon. It has been shown here that this source model accurately represents the dynamic displacement field resulting from the AE event. Unfortunately there is still no independent verification that the moment tensor representation adequately models the actual dynamic microfracture mechanisms in a heterogeneous material such as mortar. Components of the model such as the "crack plane" may not correctly represent the actual fracture process. Despite the shortfalls, however, this analysis has been shown to be a valuable tool to evaluate the fracture properties of mortar.

It should be noted that previously published two dimensional analyses of microcracking in mortar and concrete specimens showed a fair number of mode I events in addition to mixed mode, and mode II events [12],[18]. The seemingly contradictory results with what was measured here can be reconciled by considering out-of-plane moment tensor components. If the two dimensional analysis is done in the x_1-x_3 plane of figure 11, an event which appears to be mode I in that plane may actually be mode II when motion in the x_2-direction is considered. This is illustrated by event number 34, highlighted in figure 11.

Summary and Conclusions

The research described herein demonstrated the usefulness of quantitative acoustic emission analysis techniques as a tool for basic fracture research of cement-based materials. The inversion of AE data is a unique method of monitoring the dynamic processes of damage evolution and crack growth. The main zones of damage were found through the locations of the AE sources. The simplified inversion technique presented here was shown to accurately model the far-field displacement transients produced from an AE event. The primary fracture mode of microcracks in the mortar specimen was found to be mode II. A small number of mixed-mode microcracks were also observed.

No mode I microcracking was observed. Although the displacement transients were independently verified, the moment tensor source representation still requires some kind of independent verification. Current research is focused on further analyzing the AE source mechanisms in cement-based materials. This research will lead to a better understanding of the fracture process zone and the mechanisms of damage growth in quasi-brittle materials.

Acknowledgments

This research was supported by a grant from the U.S. Air Force Office of Scientific Research under a program managed by Dr. Spencer T. Wu. Additional support was provided by the NSF Center for Science and Technology of Advanced Cement-Based Materials. The SEM micrograph was made with the assistance of Mr. Todd Bergstrom.

References

[1] Aki, K. and P.G. Richards, **Quantitative Seismology**, W.H. Freeman and Company, New York, 1980, chapters 2-4.

[2] ASTM E1106-86, "Standard Method for Primary Calibration of Acoustic Emission Sensors," Annual Book of ASTM Standards, Vol. 03.03, ASTM, Philadelphia, 1986, pp. 949-969.

[3] Enoki, M. and T. Kishi, "Theory and Analysis of Deformation Moment Tensor Due to Microcracking," *International Journal of Fracture*, **38**, 1988, pp. 295-310.

[4] Hsu, N.N., J.A. Simmons, and S.C. Hardy, "An Approach to Acoustic Emission Signal Analysis," *Materials Evaluation*, **35**, 1977, pp. 100-106.

[5] Hsu, N.N. and F.R. Breckenridge, " Characterization and Calibration of Acoustic Emission Transducers," *Materials Evaluation*, **39**, 1981, pp. 60-68.

[6] Hsu, N.N., "Dynamic Green's Functions of an Infinite Plate - A Computer Program," Report NBSIR 85-3234, National Bureau of Standards, Gaithersburg, MD, 1985.

[7] Jia, Z.L. and S.P. Shah, "Two Dimensional ESPI and Concrete Fracture Mechanics," Presented at the SEM-ASNT Fall Conference, November 16-20, 1992, Chicago, Illinois.

[8] Kim, Y.K., and W. Sachse, "Characteristics of an Acoustic Emission Source from a Thermal Crack in Glass," International Journal of Fracture, **31**, 1986, pp. 211-231.

[9] Landis, E., C. Ouyang, and S.P. Shah, "Automated Determination of First P-Wave Arrival and Acoustic Emission Source Location," *Journal of Acoustic Emission*, **10**, 1992, pp. S97-S103.

[10] Lange, D.A., "Relationship Between Microstructure, Fracture Surfaces, and Material Properties of Portland Cement," Ph.D. Dissertation, Department of Civil Engineering, Northwestern University, Evanston, Illinois, 1991.

[11] Li, Z., S. Kulkarni, and S.P. Shah, "Application of AE Technique in Measurement of Fracture Properties of Unnotched Concrete Specimens," Presented at the SEM-ASNT Fall Conference, November 16-20, 1992, Chicago, Illinois.

[12] Maji, A.K., C. Ouyang, and S.P. Shah, "Fracture Mechanisms of Quasi-Brittle Materials Based on Acoustic Emission," Journal of Materials Research, **5**, 1990, pp. 206-217.

[13] Malvern, L.E., **Introduction to the Mechanics of a Continuous Medium**, Prentice-Hall, Inc., Englewood Cliffs, New Jersey, 1969.

[14] Miller, R.K, and P. McIntire, editors, *Nondestructive Testing Handbook, Volume 5, Acoustic Emission Testing*, 2nd. Ed., ASNT, 1987.

[15] Michaels, J.E. and Y.-H. Pao, "The Inverse Source Problem for an Oblique Force on an Elastic Plate," *Journal of the Acoustical Society of America*, **77**, 1985, pp. 2005-2011.

[16] Michaels, J.E. and Y.-H. Pao, "Determination of dynamic Forces from Wave Motion Measurements," *Journal of Applied Mechanics*, **53**, 1986, pp. 61-68.

[17] Mindess, S., "The Fracture Process Zone in Concrete," *Toughening Mechanisms in Quasi-Brittle Materials*, S.P. Shah (ed.), Kluwer Academic Publishers, Dordrecht, Netherlands, 1991, pp. 271-286.

[18] Ouyang, C., E. Landis, and S.P. Shah, "Damage Assessment in Concrete Using Quantitative Acoustic Emission," *Journal of Engineering Mechanics*, **117**, 1991, pp. 2681-2698.

[19] Ohtsu, M. and K. Ono, "AE Source Location and Orientation of Tensile Cracks from Surface Observation," *NDT International*, **21**, 1988, pp. 143-150.

[20] Press, W.H., B.P. Flannery, S.A. Teukolsky, and W.T. Vetterling, **Numerical Recipes**, Cambridge University Press, New York, 1986, pp. 521-528.

[21] Scruby, C.B., K.A. Stacey and G.R. Baldwin, "Defect Characterization in Three Dimensions by Acoustic Emission," *Journal of Physics D: Applied Physics*, **19**, 1986, pp. 1597-1612.

[22] Simmons, J.A., "Deconvolution for Acoustic Emission," *Review of Progress in Quantitative Nondestructive Evaluation*, **5A**, D.O. Thompson and D.E. Chimenti, (eds.), Plenum Press, NY, 1985, pp. 727-735.

[23] Swartz, S.E., and Go, C.G., "Validity of Compliance Calibration to Cracked Concrete Beams in Bending," Experimental Mechanics, **24**, 1984, pp. 129-134.

List of Figures

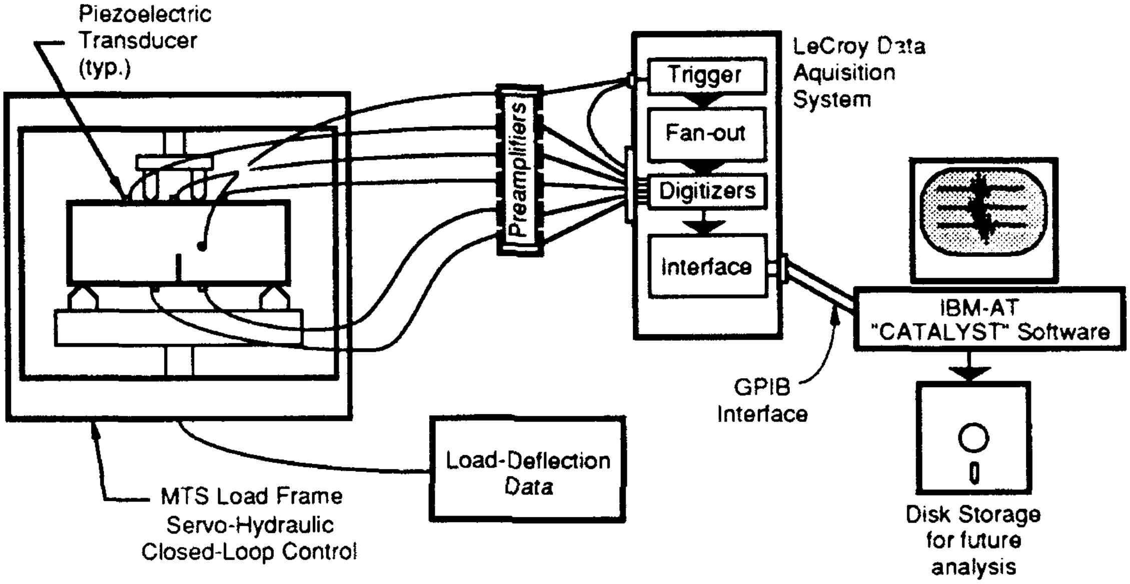
Piezoelectric
Transducer
(typ.)
Preamplifiers
LeCroy Data
Aquisition
System
Trigger
Fan-out
Digitizers
Interface
IBM-AT
"CATALYST" Software
GPIB
Interface
Disk Storage
for future
analysis
Load-Deflection
Data
MTS Load Frame
Servo-Hydraulic
Closed-Loop Control

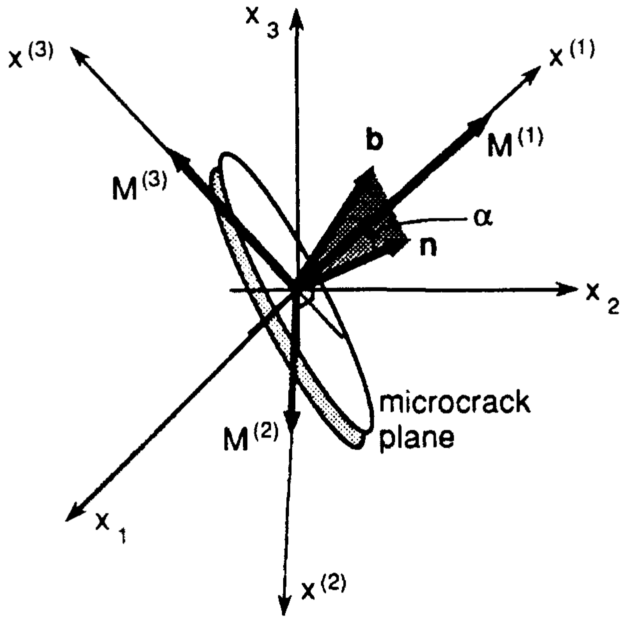

x_3
$x^{(3)}$
$x^{(1)}$
b
$M^{(1)}$
$M^{(3)}$
α
n
x_2
microcrack plane
$M^{(2)}$
x_1
$x^{(2)}$

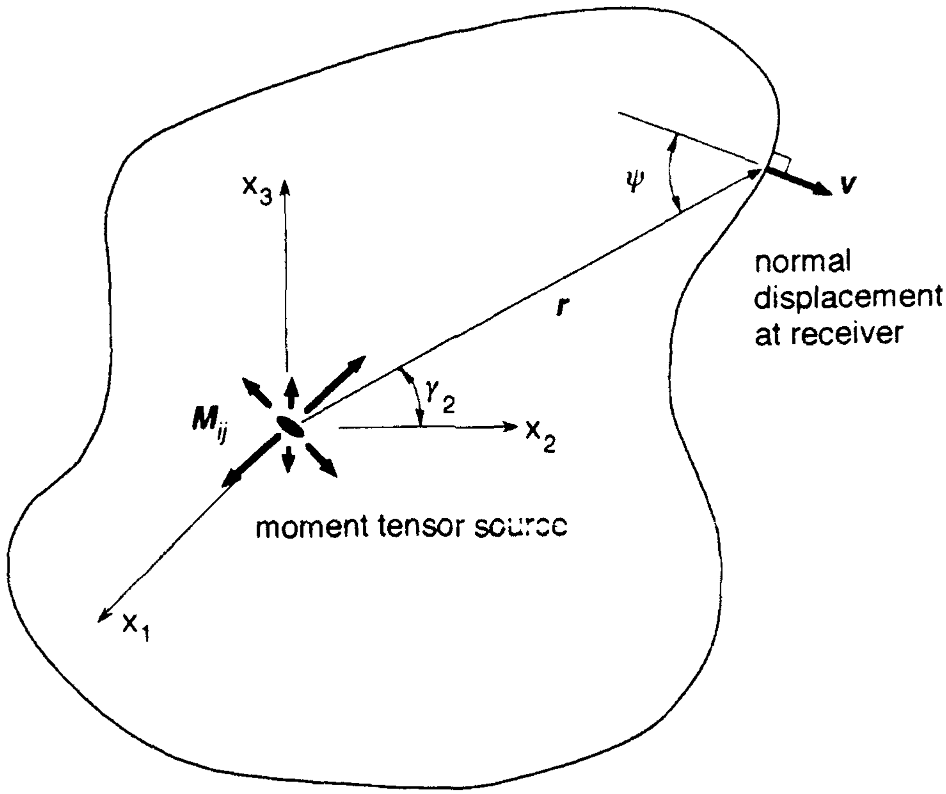

x_3
ψ
v
normal
displacement
at receiver
r
γ_2
M_{ij}
x_2
moment tensor source
x_1

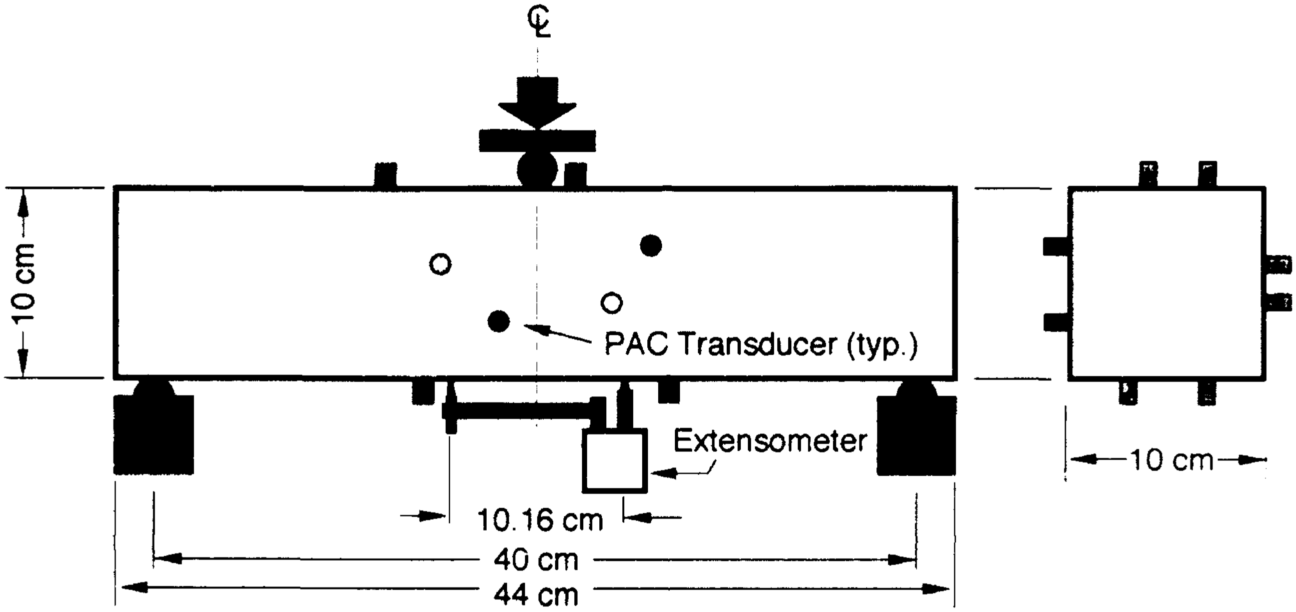

℄
10 cm
PAC Transducer (typ.)
Extensometer
10.16 cm
40 cm
44 cm
10 cm

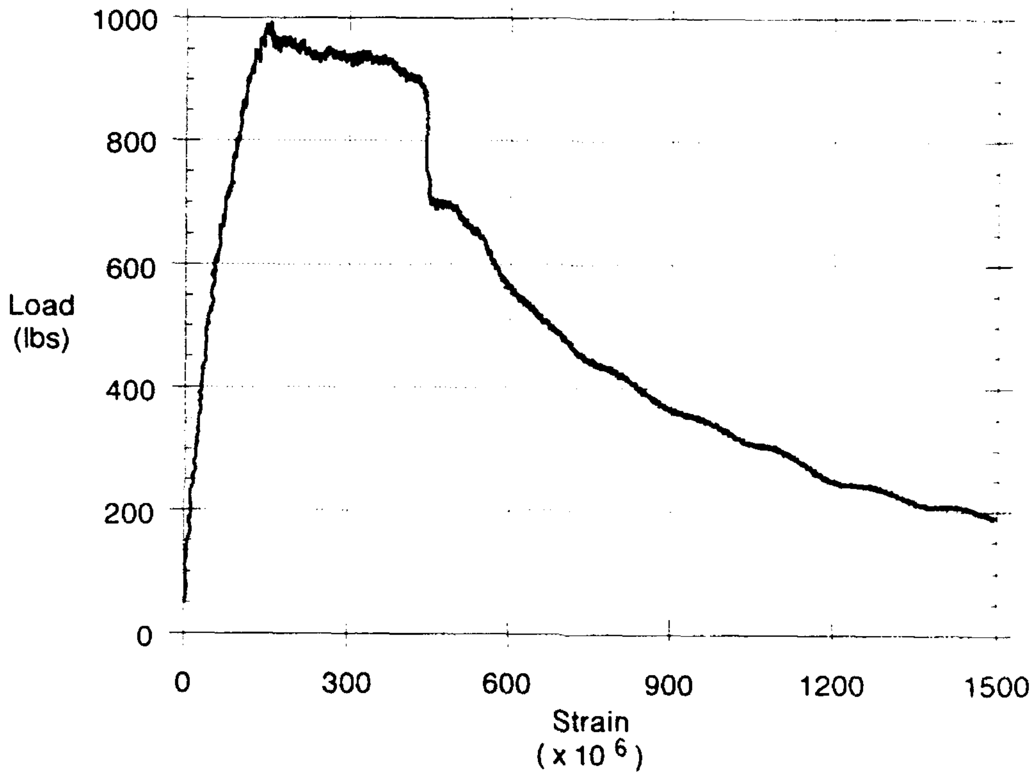
1000
800
600
400
200
0
Load
(lbs)
0
300
600
900
1200
1500
Strain
(x 10 6)

FIG 5

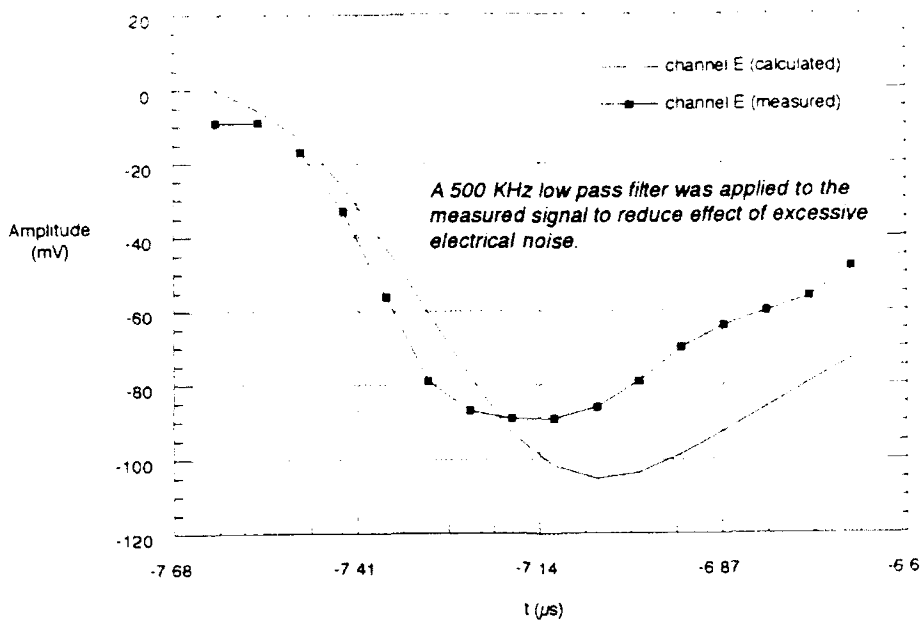

channel E (calculated)
channel E (measured)
A 500 KHz low pass filter was applied to the measured signal to reduce effect of excessive electrical noise.
Amplitude (mV)
20
0
-20
-40
-60
-80
-100
-120
-7 68
-7 41
-7 14
-6 87
-6 6
t (μs)

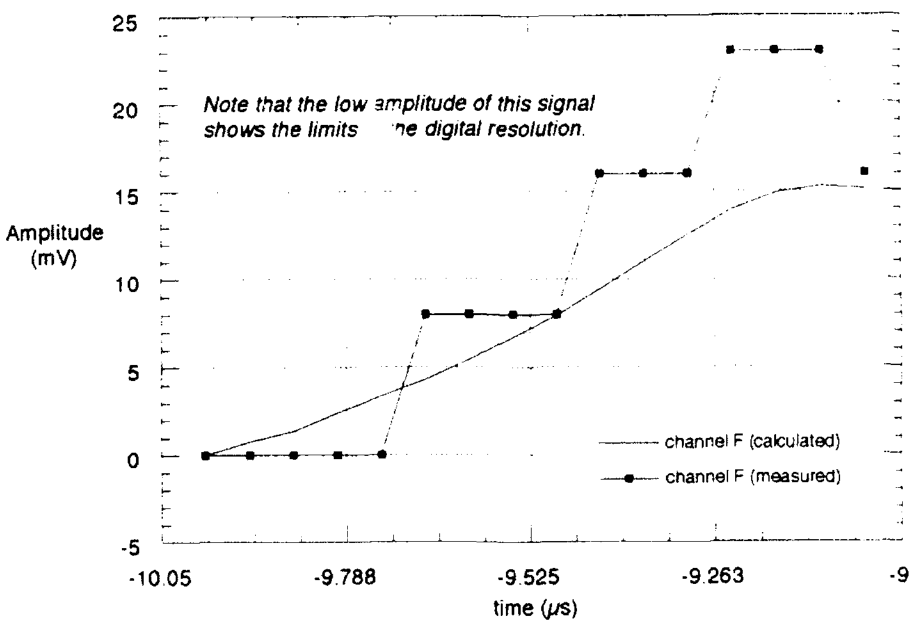

Note that the low amplitude of this signal shows the limits ne digital resolution.
Amplitude (mV)
25
20
15
10
5
0
-5
-10.05
-9.788
-9.525
-9.263
-9
time (μs)
channel F (calculated)
channel F (measured)

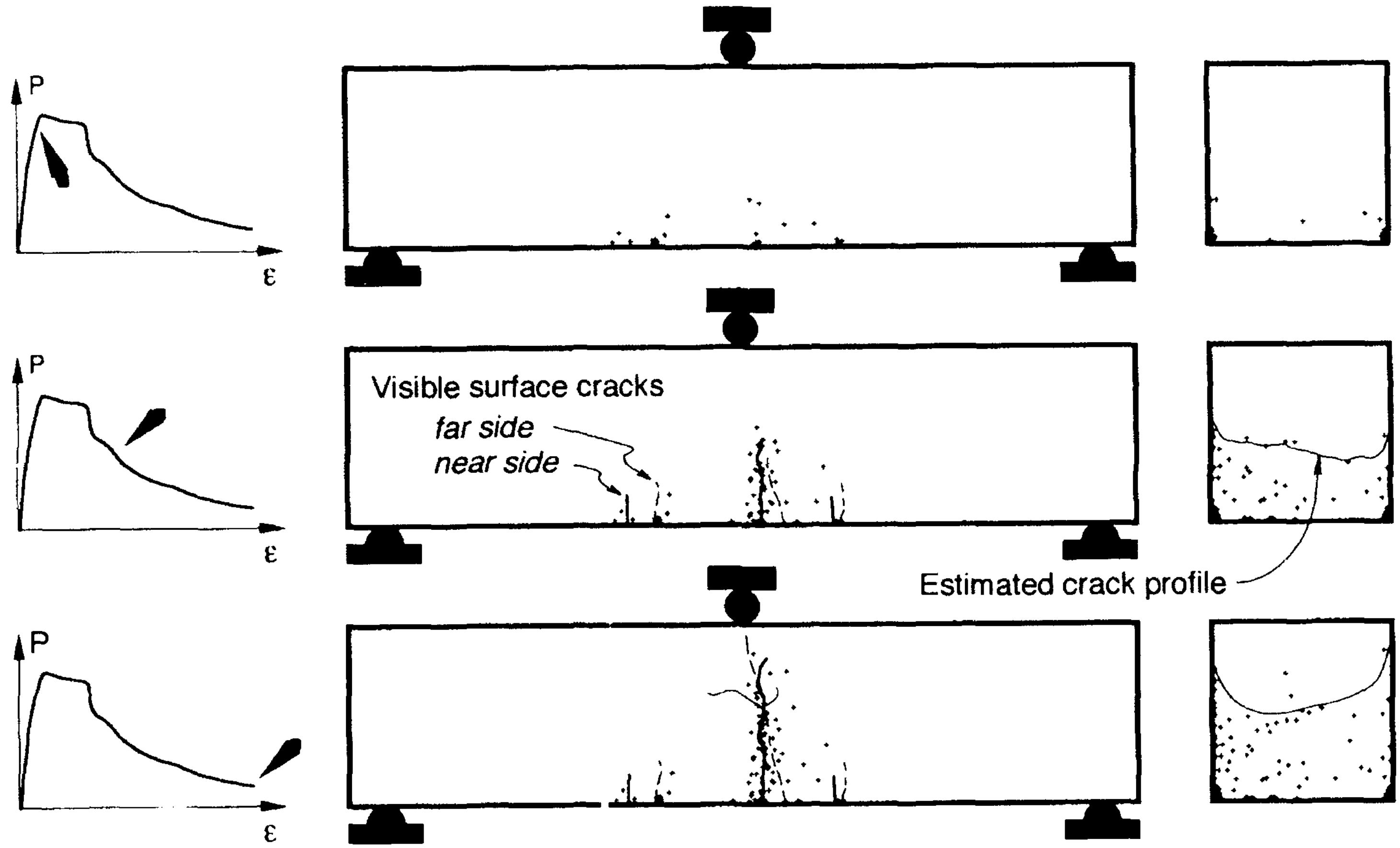
P
ε
P
ε
P
ε
Visible surface cracks
far side
near side
Estimated crack profile

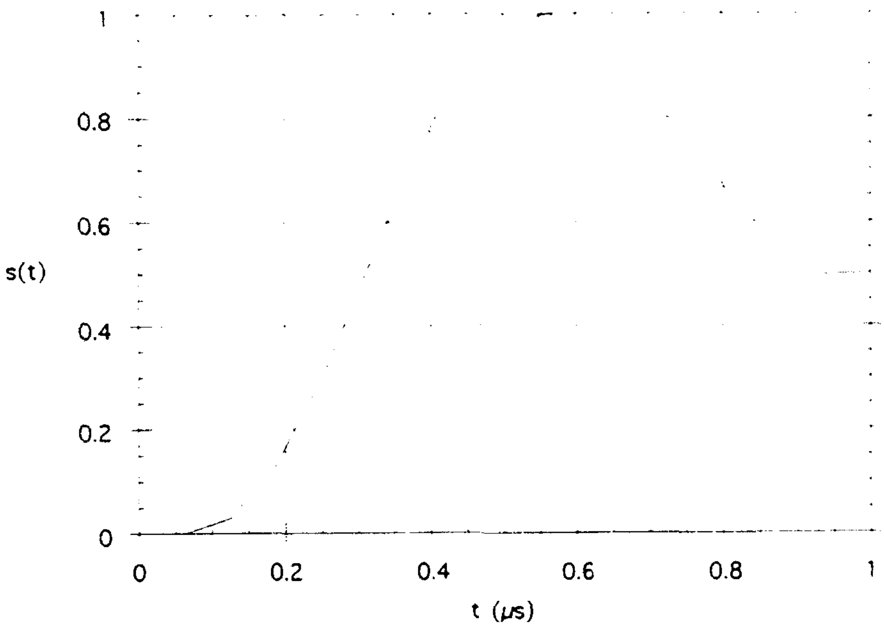
s(t)
t (μs)
0
0.2
0.4
0.6
0.8
1

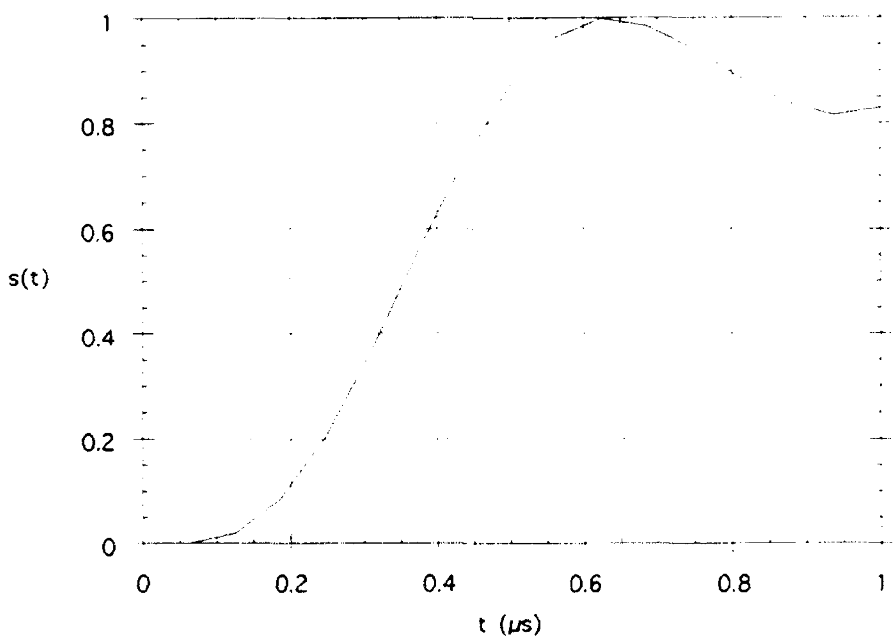
s(t)
t (μs)
0
0.2
0.4
0.6
0.8
1

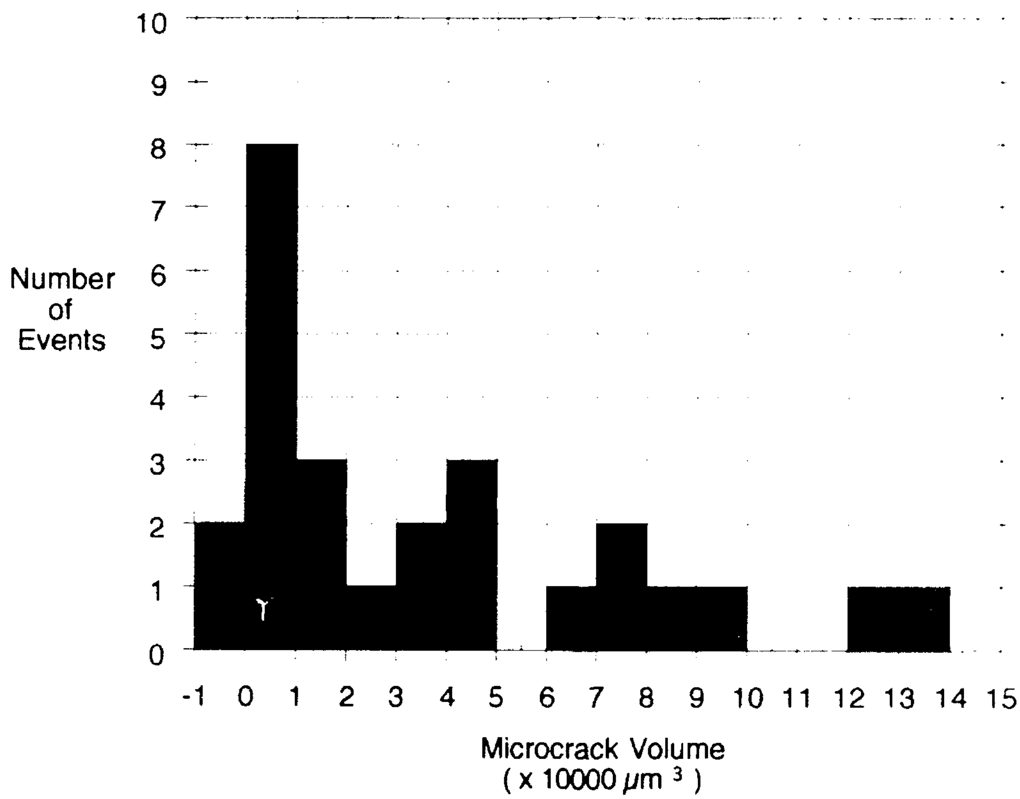

10
9
8
7
6
5
4
3
2
1
0
Number
of
Events
-1 0 1 2 3 4 5 6 7 8 9 10 11 12 13 14 15
Microcrack Volume
(x 10000 μm ³)

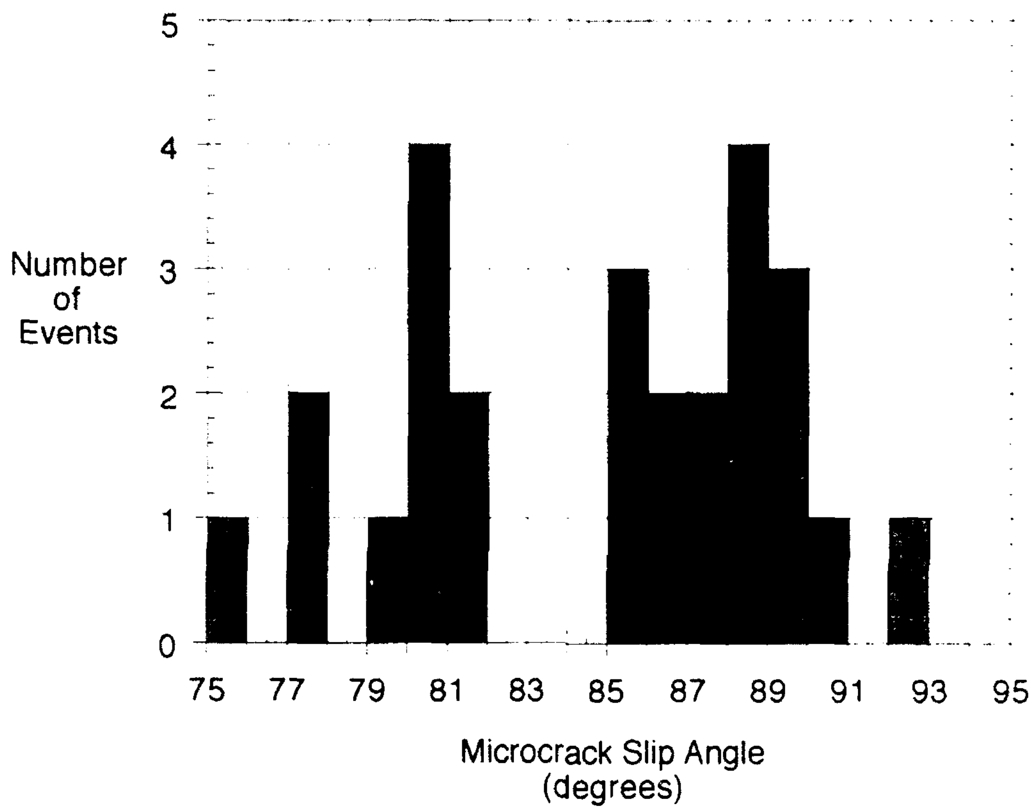

Number of Events
Microcrack Slip Angle (degrees)
0
1
2
3
4
5
75
77
79
81
83
85
87
89
91
93
95

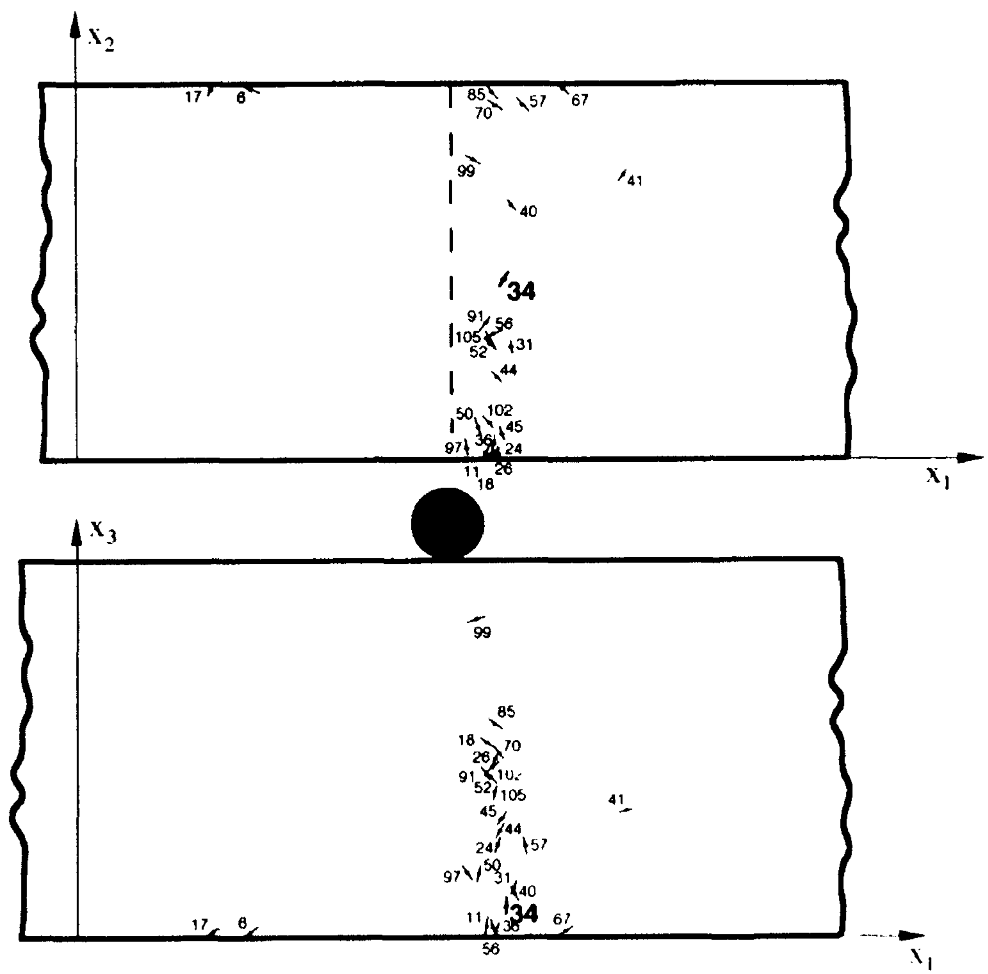

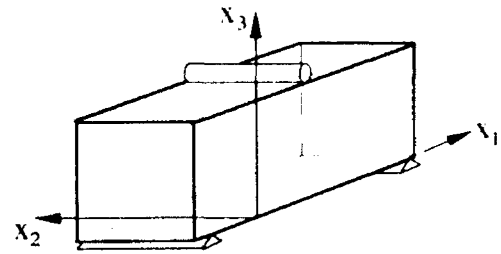

Axis Orientations

The number along side of microcrack indicates the AE event number.

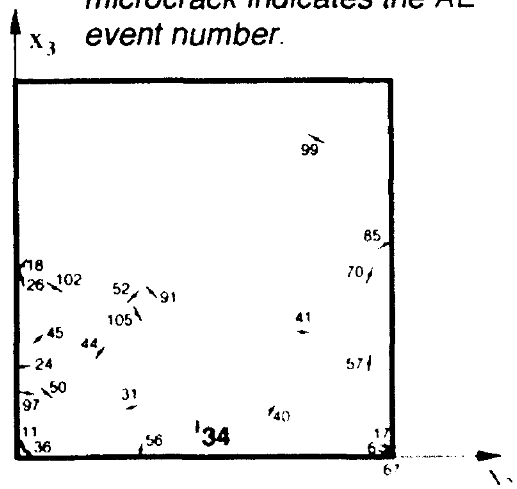

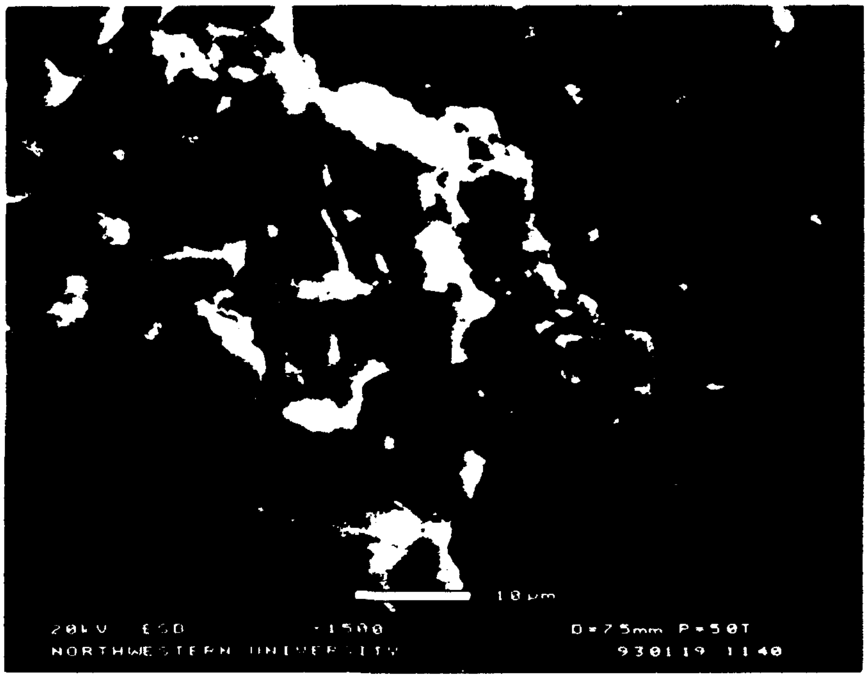
10 µm
20kV ESD x1500 D=7.5mm P=50T
NORTHWESTERN UNIVERSITY 930119 1140

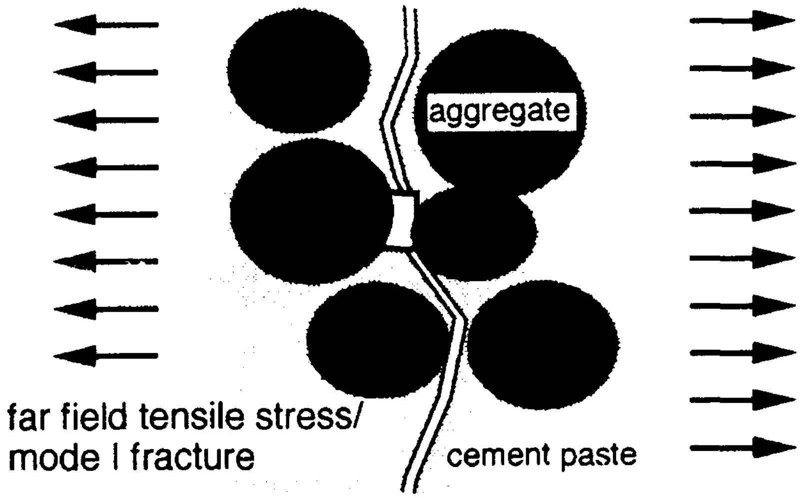
aggregate
far field tensile stress/
mode I fracture
cement paste

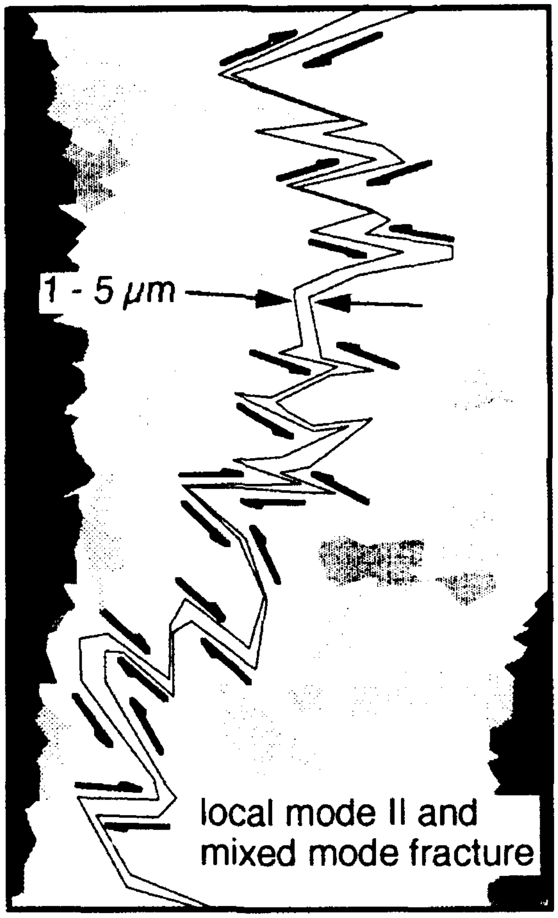
1 - 5 μm
local mode II and
mixed mode fracture

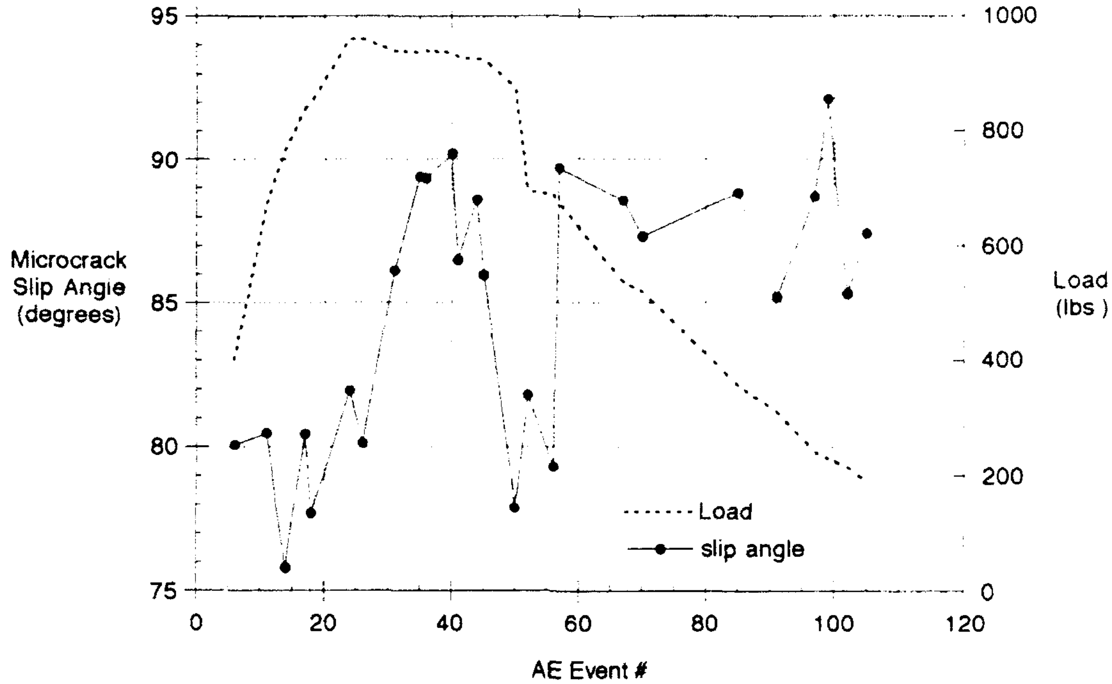
Microcrack
Slip Angle
(degrees)
95
90
85
80
75
0
20
40
60
80
100
120
AE Event #
1000
800
600
400
200
0
Load
(lbs)
Load
slip angle

Fig 14

Appendix B

Localization of microcracking in concrete under uniaxial tension

Zongjin Li[1] and Surendra P. Shah[2]

SYNOPSIS

The localization of microcracks in unnotched concrete specimens under uniaxial tension has been studied using acoustic emission (AE) analysis techniques. A new method was developed to locate the source of the AE events. It was found that the AE events started to concentrate on a narrow band of the specimen when load reached about 80% of the peak value. The macro deformation of the specimen was also monitored by using four LVDTs which were uniformly distributed along the direction of tension. Based on the experimental observations, the relationship between occurrence of AE event (microcracking) and macro deformation was further investigated. It was found that the localization of micro-cracks controlled the development of the macro crack in the specimen.

Key words: microcrock, uniaxial tension, acoustic emission, localization, fracture process.

INTRODUCTION

The microcrack localization in concrete has become an interesting topic recently partly due to the demand of understanding of the fracture process. The earlier test reported by Gopalaratnam and Shah[1] and Eligehausen et al[2]. have demonstrated the existence of localization in the strain field. Stress-strain relationship were shown to be dependent on the gauge length.

---

[1] Graduate research assistant, ACBM Center, Northwestern University, Evanston, IL 60208

[2] Professor of Civil Engineering, Director of NSF ACBM Center, Northwestern University, Evanston, IL 60208.

However, the data concerning the occurrence and development of microcracks as well as fracture process zone available from these test are limited due to the limitation of the measuring instrument such as strain gauge and displacement transducers.

Based on the evaluation of the fracture energy of brittle materials, Schorn[3] inferred that the damage process might be divided into three sections: the formation of a microcrack (the cracking process start at a load about 40% of the peak load), the accumulation of microcracks and the propagation of a macrocrack (at a critical point in the descending branch of stress-strain curve). However, there was no experimental verification in terms of microscopic observations of fracture process. Raiss, M.E., Dougill, J. W. and Newman[4] conducted uniaxial tension test using a closed loop servo-controlled machine with the help of the parallel steel bar load-sharing system. Moire interferometry technique was adopted to examine the full field surface strain. They observed that localization in the strain field occurred prior to the attainment of the maximum load. They concluded that the load-extension relationship is not a property of the bulk material but is strongly influenced by behavior local to the fracture process zone. The fracture of concrete is characterized by the formation and propagation of fracture process zones. It has been suggested that these zones are initially formed by microcracks which subsequently coalesce to the fracture process zone. Since Moire interferometry technique can only measure the surface deformation, no information is available for the occurrence of internal microcracks.

Due to the capability of detecting the activity of internal microcracking, AE technique has been employed to study damage and microcrack nucleation in a stressed material for many years[5]. The rate and sum of occurrence of AE activity have been used to predict the extent of internal damage of concrete[6]. Maji and Shah[7,8] applied AE technique to detect the fracture process zone for cementitious composite. Kim and Koo[9] correlated the AE event and crack pattern of reinforced concrete beams to examine flexural failure. Maji, Ouyang and Shah[10] discussed some basic aspects on applying AE to cement-based materials, and used the moment tensor approach to characterize the properties of a microcracking of center-cracked concrete plate. Landis and Shah[11] recovered the microcrack parameters for mortar beam specimen using quantitative acoustic emission technique.

Berthaud et al.[12] carried out tensile test on concrete with the application of acoustic emission together with replica techniques to observe microcracking. They found that the propagation of a single macrocrack is always surrounded by a damaged zone and the cracking (acoustic activity) was uniform in this zone. Their AE map showed that as early as at 74 percent of peak load two different zones of cracking occurred simultaneously. The heavy localization was observed at 93 percent of load. It should be indicated that since two lateral surfaces of the specimen were fully glued on metallic bars with epoxy resin and the load was transferred through shear along entire loading dimension of the specimen in their test, it is possible to get some AE events caused by surface debonding.

Mihashi et al.[13] applied three-dimensional acoustic emission technique to study double cantilever beam response. The test revealed that fracture process zone did have a 3-D structure. According to their results, microcracking may not prevail at the region close to the specimen's surface but randomly occur around main crack.

The objective of the present study was to evaluate the relationship between microcracking and macroscopic deformation. A series of uniaxial tension tests were carried out on both plain concrete and fiber reinforced concrete specimens. A stable post-peak response was obtained with a closed-loop digitally controlled testing equipment. Specimens were not notched and no load-sharing system was used. The microcrack nucleation was detected using an AE measurement system, and macroscopic deformation was measured by LVDTs. The AE events obtained during tests were analyzed and the source location and the characteristics of the microcracks were deduced. These characteristics were used to explain the macro behavior of the material and to show that the localization of microcracks was the primary mechanism that controls the behavior of the macro deformation.

RESEARCH SIGNIFICANCE

This paper reports the results of the investigation of the phenomena of the localization of microcracking in concrete under uniaxial tension. The uniaxial tests were conducted by using a newly developed interchangeably multiple channel control method on unnotched concrete specimen to obtain the stable post peak response. An acoustic emission measurement system with six channels was used in the investigation to detect the occurrence of microcracking. It was found that the degree of the internal damage could be indicated by the rate of the occurrence of AE events. The experimental results also shown that the microcracking localization did exist and occurred before peak load. The location of optically observed macrocrack as well as the change in macroscopic deformation pattern were largely controlled by the nucleation of the microcracking.

EXPERIMENTAL DETAILS

Preparation of the specimen

Three types of specimens-- plain concrete, steel fiber reinforced concrete (SFRC) and polypropylene fiber reinforced concrete (PFRC) were prepared. The test program is shown in

Table I. The plain concrete specimens were prepared using a mix proportion of 1 : 0.65 : 2.6 : 2.6 (cement : water : sand : coarse aggregate) by weight. The maximum size of aggregate was about 13 mm. The SFRC specimens were prepared using a proportion of 1 : 0.6 : 2.45 : 2.45. 0.5% by volume of hooked steel fibers manufactured and provided by Bekaert Corp. were added into the mixture. In addition, superplasticizer (1.7 ml per pound of cement) was added to achieve reasonable workability. The PFRC specimens were prepared with a mix proportion of 1 : 0.56 : 2.4 : 2.4. Polypropylene fibers (0.5% by volume) provided by Fibermesh company together with a superplasticizer in the amount of 1.7 ml per pound of cement were added into the mixture. All the specimens were de-molded 24 hours after casting and left in a water bath for curing The specimens were tested at the age of 28 days. Two days before testing, the specimens were taken out of the bath and left to dry. Steel loading plates (end tabs) were then glued to the ends of the specimens. Before gluing the loading plates, both the specimen surface and the steel plates were polished with #400 sand paper and cleaned with acetone. The details of gluing specimens are provided elsewhere[14]. The entire specimen size was 13 X 5 X 1.1 in. After gluing the loading plates, the test portion left was 5 X 5 X 1.1 in.

Test setup

The set-up for the test is shown in Fig. 1. Two identical loading fixtures were used: one mounted on the machine's actuator and the other connected to the load cell. In each fixture, a sliding steel block was provided which helped to center the specimen. This kind of set-up provides boundary conditions close to those provided by non-rotatable loading platens[15]. The thickness of the loading plate was gradually reduced (Fig. 1) from 3/8" to 1/16" to avoid a sudden change in stiffness and consequent stress concentration. Four LVDTs with a working range of

0.025" and gage length of 2.75" were mounted on the specimen (Fig. 1). The signals from the LVDTs, the stroke LVDT and the load cell were acquired using LabTech Notebook software. The readings of all six sensors were displayed in six individual windows (sensor reading as a function of time) on the Notebook screen. These graphs were useful in making decisions regarding switching of the control mode among those LVDTs. Six PZT transducers were also glued (Fig. 1) on the surface of the specimen to monitor the acoustic emission (AE) activity. The AE events were mainly monitored from the central 127 mm X 127 mm (5 in. X 5 in.) area of the specimen.

AE Measurement system

The AE measurement system shown in Fig. 2 was used to acquire AE data during the test. The system consisted of transducers, preamplifiers and A-D modules. Six channels were employed. The transducers were purchased from Physical Acoustics Corporation (model micro 80). These general purpose transducers are made of piezoelectric crystal and are hence called PZT transducers. They are convenient to use because of their small size (9.5 mm diameter and 11.1 mm height), negligible weight (5 g) and desirable sensitivity. These transducers have an essentially flat amplitude response of approximately ± 9 dB in the frequency range of 100 kHz to 1.2 MHz. It was found by calibration that these PZT transducers measure surface velocity of a material during the period of first P-wave (Maji et al., 1989)[16]. The preamplifiers used were also purchased from Physical Acoustics Corporation (model number 1220B). This preamplifier has a bandwidth of 20-1200 kHz and a gain of 40 or 60 dB (interchangeable). In the system, channel A was used as a trigger channel and was connected to a 6103 amplifier trigger module. The other five channels were used as working channels and were connected to five TR8837F digitizer modules. A 6128 fan-out module was used to receive the signal from 6103 amplifier and to trigger all working channels simultaneously. A LECROY 8901A interface board was used to communicate with an IBM-AT via a GPIB cable. The operation of LECROY system was controlled by Physical Acoustics' CATALYST program which also stored the digitized data on the computer's hard disk. 3000 data points were stored for each channel at a digitizing rate of 16 MHz.

Test procedures

The uniaxial tension tests were carried out by using a new test method[14] in which a digitally controlled closed-loop MTS testing machine, five individual control channels and a strategy of continuous switching of control mode to catch the formation of the major crack were employed. The specimen was first loaded under stroke control at a rate of 0.00156 mm of piston displacement per minute. While loading, the output of the LVDTs and load cell were monitored by using the Notebook program. With the load increasing, the slope of the curve of the output of LVDTs vs. time exhibited some differences. The test mode was then switched to LVDT control by choosing the LVDT having the steepest slope of the output. Usually, the first change of the control mode to an LVDT mounted on specimen is not sufficient to guarantee that the major crack could be caught. To ensure the softening response measurement, the control mode had to be changed frequently in accordance with the current time-rates of the output of the LVDTs.

TEST RESULTS

Occurrence of AE events

The stress versus deformation (measured by the control LVDT) relationships are plotted in

Fig. 3-5 for a plain concrete specimen, a SFRC specimen and a PFRC specimen, respectively. These figures are superimposed with the occurrence of the AE events. Generally speaking, the first AE event usually is noticed earlier for plain concrete specimen as compared to the specimens of fiber reinforced. In the pre-peak load region, the rate of the occurrence of the AE events shows an obvious change around the 80 percent peak load. This phenomenon is also clearly demonstrated in the AE event accumulation curves for specimen C-2 as shown in Fig. 6 where the slope of the curve become much steeper around 0.8 peak load. A quite similar trend was also observed for other specimens. The rate of the occurrence of AE event is, therefore, a strong indication of the internal damage and the value of 0.8 peak load can be used as a stage transferring point.

It also should be indicated that in the post peak region, the fiber reinforced concrete specimens usually have more nucleation of AE event than plain concrete specimens do. This phenomena could be attributed to the fiber debonding and matrix microcracking.

Some basic features of the measured AE signal

The AE signal was first analyzed by using the FFT transform to examine the frequency distribution of the microcracking. A typical result is shown in figure 7. Two response peaks are shown in the figure. One is with a central frequency about 100 KHz and another with a central frequency of 330 KHz. A statistical evaluation for 164 AE signals of a concrete specimen shows that the mean for second peak is 322.93 KHz with a standard derivation of 16.33 KHz and the mean for the first peak is about 113.75 KHz with a standard derivation of 15.93 KHz. These observations are quite consistent with most AE signals recorded for other specimens. It should be indicated that these frequency values agree with the findings of Reymond[17], Labuz, Shah and

Dowding[18] and Kim[19]. They reported a observation for a frequency range of 250 to 500 KHz for rock and concrete acoustic emission. If we assume that the second peak represents the longitudinal wave and the first is for shear wave, the length for longitudinal and shear wave can be estimated by using the formula:

$$\Lambda = \frac{C}{f} \tag{1}$$

where C is either velocity of longitudinal wave or velocity of shear wave and f is the corresponding frequency. After knowing the wavelength, the wave number can be obtained by using the formula:

$$K = \frac{2\Pi}{\Lambda} \tag{2}$$

The calculated results of wave length are 12.3 mm (0.486 in.) and 21.8 mm (0.86 in.) for P-wave and shear wave, respectively. The wave number for P-wave and shear wave determined from equation 2 are 0.51 1/mm (12.93 1/in.) and 0.287 1/mm (7.3 1/in.), respectively. These values are useful in determining the geometry of the specimen. Since transducers have to be located far from the AE source to discern the shear wave component from the first few arrival waves, the size of the specimen should be large enough. The far field condition has been defined by Aki and Richards[20] as:

$$\begin{gathered} \frac{2\Pi r}{\Lambda} >> 1 \\ r >> \frac{\Lambda}{2\Pi} \end{gathered} \tag{3}$$

Where, r is the distance between AE source and transducer. Once the wave length is known, the minimum requirement can be easily estimated from equation 3. For instance, if we use the value of the wave length obtained in this section, the minimum dimension of the specimen would be few inches.

AE source location

The AE source location can be deduced by using the differences among the first P- wave arrival times at each of the AE transducers. To get the better estimate of the first P-wave arrive time, the AE signals were smoothed by using a band pass filter. The range of the frequency for pass-band is from 80 KHz to 350 KHz. It seems that the band filter is essential for sharpening the first arrived P-wave.

A complete set of filtered AE signals is plotted in Fig. 8. It can be seen from the figure that arrival times of the first P-wave are different for the transducers at different locations. Once the differences in arrive times are calculated, for a two dimension case, we can write the error between the distance from transducer 1 to the AE source and the distance from transducer i to the AE source as:

$$e_{1i} = \sqrt{(x-x_1)^2+(y-y_1)^2}-\sqrt{(x-x_i)^2+(y-y_i)^2}-\Delta t_{1i}C \qquad (4)$$

Where, x and y are coordinates of the AE source to be determined and x_1 (x_i) and y_1 (y_i) are the coordinates of the transducers. Δt_{1i} represents the difference of arrive time between transducer 1 and i (i=2,3,...,n) and C is the P-wave velocity. For an ideal situation, the error expression should be zero and the AE source location should be easily determined by an intersection of two set of equations. However, for a real experiment, error always exists. In order to minimize the test error, following method is developed. First, the square of individual error is summed up:

$$e = \sum_{i=2}^{n} (e_{1i})^2 = \sum_{i=2}^{n} (d_1 - d_i - \Delta t_{1i} C)^2 \tag{5}$$

Where,

$$d_1 = \sqrt{(x-x_1)^2+(y-y_1)^2}$$
$$d_i = \sqrt{(x-x_i)^2+(y-y_i)^2} \tag{6}$$

Then, the total error is differentiated with respect to x and y. We get:

$$f_1(x,y,C) = \frac{\partial e}{\partial x} = 2\sum_{i=2}^{n}\left(\frac{x-x_1}{d_1} - \frac{x-x_i}{d_i}\right)(d_1 - d_i - \Delta t_1 iC) \tag{7}$$

and

$$f_2(x,y,C) = \frac{\partial e}{\partial y} = 2\sum_{i=2}^{n}\left(\frac{y-y_1}{d_1} - \frac{y-y_i}{d_i}\right)(d_1 - d_i - \Delta t_{1i} C) \tag{8}$$

By setting $f_1(x,y,C)$ and $f_2(x,y,C)$ equal zero, the values of x and y can be solved by employing a numerical method provided that the value of wave velocity is known. Moreover, if the error equation is differentiated with respect to wave velocity, C, we get,

$$f_3(x,y,c) = \frac{\partial e}{\partial C} = 2\sum_{i=2}^{n} \Delta t_{1i}(\Delta t_{1i}C + d_i - d_1) \tag{9}$$

It should be pointed out that solving equations 7, 8, and 9 together will provide not only the source location but also the wave velocity.

The maps of the AE event source location for a plain concrete specimen C-3 is plotted in Fig. 9. This figure shows the AE events recorded prior to 80 percent of peak load, (Fig. 9 a), the AE events those occurred between 80 percent of peak load prior to the peak and 80 percent peak load after the peak (Fig. 9 b) and the AE signals recorded after 80 percent of the post-peak load (Fig. 9 c). It is obvious that the AE map for the first period demonstrated a random distribution (Fig. 9 a). The majority of AE events registered in the period between 0.8 pre-peak load and 0.8 post peak load showed a trend to localize on a narrow band of the specimen as shown in Fig. 9 b. It should be noted that the later registered microcracks (AE events which occurred in the period after 0.8 post peak load) primarily occurred along this narrow region which always coincided with the position of the major crack as shown in Fig. 10. It also should be mentioned that although the early registered microcracks appeared to have a random distribution, their influence on the macro deformation is quite obvious as discussed later.

It should be noted that sometimes there were more than one cluster of microcracking occurring during the loading history. However, the cluster which formed in early loading stage does not play an important role in the formation of major crack. In contrast, the narrow region which appeared around 0.8 pre peak load directly correlated with the formation of the major crack. Fig. 11 shows the AE event location for plain concrete specimen C-2. It can be seen from Fig. 11 (a) that the first few micro-cracks all registered around a small area at the bottom, showing a trend of localization. However, as the load increased, addition microcracks were registered and one more cluster formed. As shown in Fig. 11 (b), the AE event generated during the period between 0.8 pre peak load and 0.8 post peak load started to concentrate on a narrow region just above the middle portion on the right side, forming another localization zone. It is shown in Fig. 12 that the major crack developed along this narrow band rather than at the location where the microcrack cluster formed in the early loading stage.

The distribution of the wave velocities obtained by solving equations (7), (8) and (9) simultaneously is plotted in figure 13. It can be seen from the figure that the shape of the distribution resembles a bell curve. The highest percentage of the computed P-wave velocity is with a range of 3048 m/s and 3556 m/s. However, the mean of the calculated velocity is 3017 m/s. It should be indicated that the values obtained by using present method is lower than P-wave values obtained by Carino et al. [21] who used two other methods: the through-transmission, pulse-velocity method (ASTM C 597) and the impact-echo method. They reported an average velocity of 4020 m/s measured using pulse-velocity method and a value of 3660 m/s obtained from impact-echo method. They had indicated that the lower velocity, which is close to the value obtained in present study, had better agreement with their nondestructive experimental measurement.

The influence of microcracks on macro deformation of a specimen

To illustrate the effect of microcracks on macro deformation, the outputs of the LVDTs during the whole loading history together with the source location of the AE event registered during different stages for a plain concrete specimen, C-1, are shown in Fig. 14-15, respectively. It can be seen from figure 14 that the outputs of the LVDTs are close to each other at the beginning portion of test. An obvious difference among the slopes of the output curves for all the LVDTs can be observed from the figure when the load reached about 80 percent peak load. This implied that the specimen did not deform uniformly. Some portion of specimen underwent a larger deformation than other parts did. This agrees with the previous observation and verified that the stress-deformation curve for the specimen is not unique as shown in Fig. 16. Thus, strictly speaking, the conventionally used stress-strain curve is not a material property. This curve is meaningful only because it describes the behavior of a weak link in the material which controls the failure mechanism of the specimen.

It is interesting to note that the differences of these LVDT's outputs (Fig. 14) is largely related to the occurrence of microcracks (Fig. 15). As shown in figure 14, the LVDT-3 and LVDT-4, which spanned the right portion of the specimen, showed a much larger output than that of LVDT 1 and 2, which covered the left portion of the specimen, at the end of stage A when the load approached 80% of the peak value. Correspondingly, the AE-event map (see Fig. 15 a) clearly shows that most microcracks registered in the same period come from the right side of the specimen. Furthermore, when the AE events started to concentrate at the right bottom portion of the specimen (see Fig. 15 b) which was spanned by LVDT-4, the reading of the LVDT continued to increase monotonically. On the other hand, the LVDT-3 first slowed the increasing rate and then changed its slope sign from positive to negative during this period. Finally, when the AE events continued to nucleate in the specimen portion covered by LVDT-4 (see Fig. 15

c), the output of the LVDT kept increasing while the others continued dropping. This implies that the macro behavior of the material significantly depends on the activity of microcracks. It should be indicated that this phenomena is quite consistent with all other specimens.

CONCLUSIONS

The behavior of the localization of concrete has been studied by employing the acoustic emission technique. The research presented here supports the following conclusions:

1) The fracture process of unnotched concrete specimen under uniaxial tension was found to involve three stages: distributed damage during loading of the sample to about 80% of pre peak load, formation of microcrack localization during loading period between 80% of pre peak load and 80% of post peak load and the major crack propagation during the period after 80% of post peak load.

2) The strain localization for a concrete specimen under uniaxial tension occurred before peak load, starting at about 80% peak value.

3) The new source location method are capable to deduce the location of AE events as well as wave velocity. The internal damage of concrete detected using AE technique has good correlation with macroscopically observed deformation.

4) The macro deformation of the concrete specimen is largely influenced by nucleation of microcracks. Hence, the moduli of the concrete (or FRC) is a function of microcracking. Due to the strain localization, the deformation of the concrete is a local rather than a global characteristic. Therefore, the so called stress-strain relationship is not a material property. The measurement of global behavior is meaningful because it reflects the behavior of the weak link

of the material.

ACKNOWLEDGEMENTS

The authors gratefully acknowledge the financial support of the U. S. Air Force of Science and Research under a program managed by Dr. Spencer T. Wu. The acknowledgement is also extended to the support from National Science Foundation Center for Science and Technology of Advanced Cement Based Materials (NSF-ACBM).

References:

1. Gopalaratnam, V. S., and Shah, S. P., "Softening response of plain concrete in direct tension", J. of the A.C.I. Proc., Vol. 82, 1985, PP 310-333

2. Eligehausen, R. and Sawade, G., "Behavior of concrete in tension", part 1 and part 2, Betonwerk and Fertigeil -- Technik, Heft 5, PP 315-322 and Heft 6, 1985, pp 389-391.

3. Schorn, H., "Strength-independent evaluation of fracture energy (GF) of brittle materials",Fracture Process in Concrete, Rock and Ceramics, Edited by J. G. M. Van Mier, J. G. Rots and A. Baker. 1991 RELIM, E. & F. N. Spon, 2-6 Boundary Row, London SE18HN, ISBN 0419 158707, pp 159-162.

4. Raiss, M. E., Dougill, J. W., and Newman, J. B., "Observation of the development of fracture process zones in concrete", Fracture of Concrete and Rock: Recent Development, Edited by S. P. Shah, 1989, pp 243-253

5. Hamstad, M. A., "A review: Acoustic emission, a tool for composite material studies", Experimental Mechanics, V. 26, 1986, PP 7-13

6. Berthelot, J. M., and Robert, J. L., "Modeling concrete damage by acoustic emission", J. of Acoustic Emission, Vol. 6, 1987, PP. 43-60.

7. Maji, A. K., and Shah, S. P., "Process zone and acoustic emission measurement in concrete", Experimental Mechanics, Vol. 28, 1988, PP 27-33.

8. Maji, A. K. and Shah, S. P., "Application of acoustic emission and laser holography to study micro-fracture in concrete", American Concrete Institute, SP-112, Nondestructive Testing, 1989, PP 83-109

9. Kim, M. K., and Koo, T. K., "Acoustic emission from reinforced concrete beams", Magazine of Concrete Research, Vol., 41, 1989, PP 229-234

10. Maji, A. K., Ouyang, C., and Shah, S. P., "Fracture mechanism of quasi-brittle material based on acoustic emission", J. of Material Research, Vol. 5, No.1, 1990, PP 206-217

11. Landis, Eric N. and Shah, Surendra P. , " Recovery of microcrack parameters in mortar using quantitative acoustic emission", Submitted to Journal of Nondestructive Evaluation, 1993.

12. Berthaud, Y., Ringot, E., and Schmitt, N., "Experimental measurements of localization for tensile test on concrete", Fracture Process in Concrete, Rock and Ceramics, Edited by J. G. M. Van Mier, J. G. Rots and A. Baker, 1991 RELIM, E. & F. N. Spon, 2-6 Boundary Row, London SE18HN, ISBN 0419 158707, 1991, pp 41-50.

13. Mihashi, H., Nomura, N. and Niiseki, S., "Influence of aggregate size on fracture process zone of concrete detected with three dimensional acoustic emission technique", Cement and Concrete Research, Vol. 21, 1991, pp 737-744

14. Li, Zongjin, Kulkarni, S. M. and Shah, S. P., "New test method for determining post peak response of concrete specimen under uniaxial tension", Accepted for publication, Experimental Mechanics, 1993.

15. Hordijk, D.A., "Local approach to fatigue of concrete," Ph.D. thesis, University of Delft, Delft, The Netherlands, 1991, p 40.

16. Maji A. K. and Shah S. P., "Application of acoustic emission and laser holography to study microstructure in concrete", ACI, SP-112, Nondestructive Testing, 1989, pp 83-109.

17. Reymond, M. C., "Acoustic emission in rocks and concrete under Laboratory conditions", Proceedings of 2nd Conference on Acoustic Emission/Micro-seismic activity in Geologic Structures and Materials, The Pennsylvania University, Pa., Trans. Tech. Publication, PP 27-34

18. Labuz, J. F., Shah, S. P. and Dowding, C. H., "The fracture process zone in granite: Evidence and effect", Inter. J. of Rock mechanics and Mining sciences Geomech. Abstr., Vol. 24, No. 4, 1987, pp 235-246.

19. Kim, G. W., "Refinements of acoustic emission measurement to deduce three dimensional rock fracture source mechanisms", Ph. D dissertation, Northwestern University, Evanston, IL, 1989

20. Aki, K. and Richard, P. G., "Quantitative seismology, theory and methods", Vol. 1, W. H. Freeman and Company, New York, N. Y., 1980.

21. Carino, Nicholas J., Sansalone, Mary and Hsu, Nelson N., "Flaw detection in concrete by frequency spectrum analysis of Impact-Echo waveforms", International Advances in Nondestructive Testing, Vol. 12, Gordon and Breach Science Publishers, S. A., U. K., 1986, pp 117-146.

Table I Test program

Specimen name	Materials	Mixing proportion	Description	Admixture
C-1	Plain concrete	C:W:S:A* 1:0.65:2.6:2.6		None
C-2				
C-3				
SFRC-1	Steel fiber reinforced concrete	1:0.6:2.45:2.45	0.5% steel fiber by volume	Superplasticizer (1.7 ml /lb cement)
SFRC-2				
SFRC-3				
PFRC-1	Polypropylene fiber reinforced concrete	1:0.56:2.4:2.4	0.5% Polypropylene fiber by volume	Superplasticizer (1.7 ml /lb cement)
PFRC-2				
PFRC-3				

* C- cement; W- water; S- sand; A- course aggregate.

Figure Legend

Fig. 1	Uniaxial tension test set-up
Fig. 2	Acoustic emission measurement set-up for tension test
Fig. 3	Stress deformation curve superimposed with acoustic emission event for specimen C-2
Fig. 4	Stress deformation curve superimposed with acoustic emission event for specimen SFRC-2
Fig. 5	Stress deformation curve superimposed with acoustic emission event for specimen PFRC-2
Fig. 6	Accumulated acoustic emission event number as a function of time for specimen C-2. The slope of the curve represents the AE event release rate.
Fig. 7	Frequency distribution of a AE signal obtained by using FFT
Fig. 8	A complete set of AE event signals after filtering. The difference among the first arrival time has been used to calculate the AE source location.
Fig. 9 (a)	AE event registered during a period between zero to pre 0.8 peak load for specimen C-3.
Fig. 9 (b)	AE event registered during a period between pre 0.8 peak load to post 0.8 peak load for specimen C-3.
Fig. 9 (c)	AE event registered during a period after post 0.8 peak load for specimen C-3.
Fig. 10	Major crack position for specimen C-3.
Fig. 11 (a)	AE event registered during a period between zero to pre 0.8 peak load for specimen C-2.

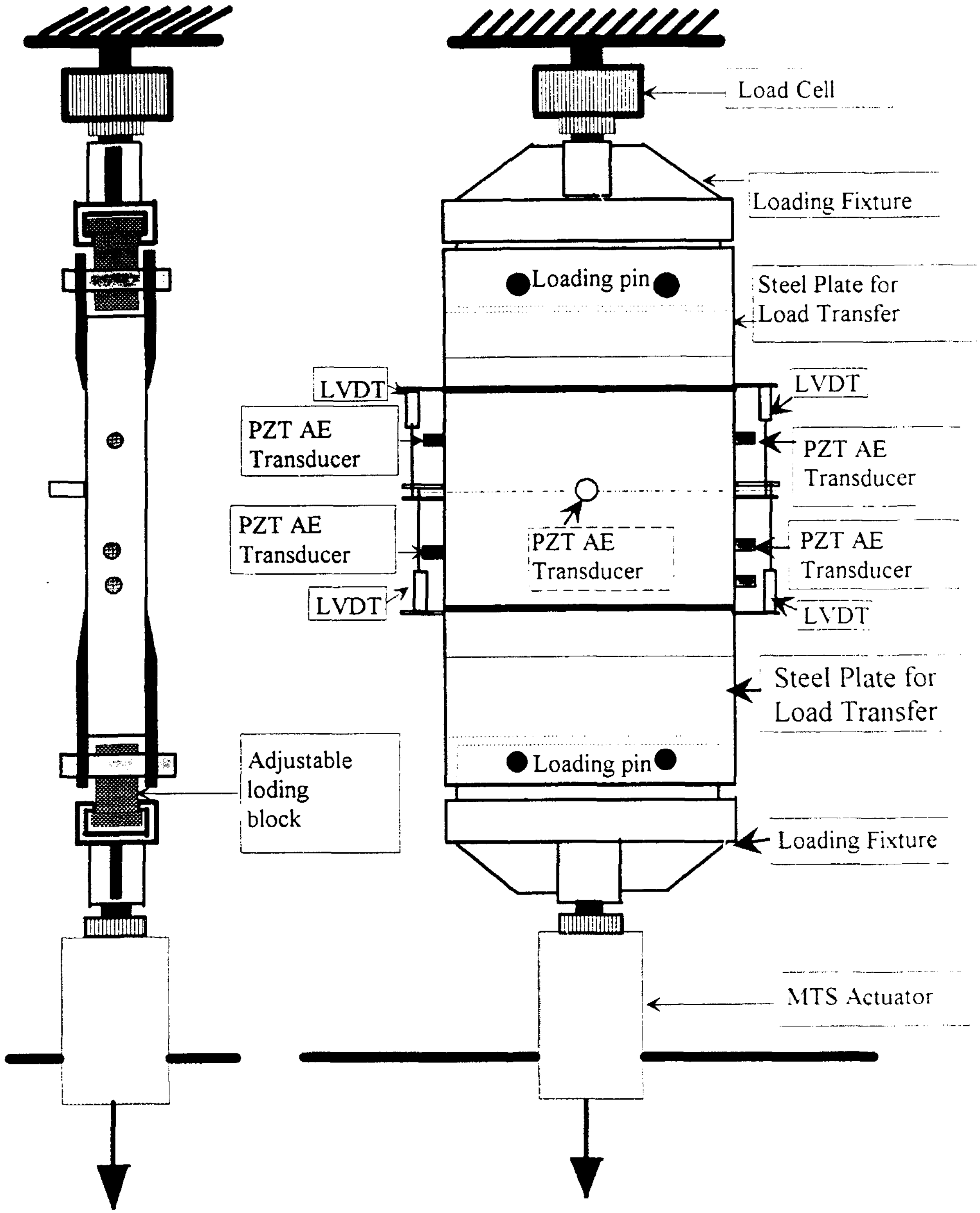

Load Cell
Loading Fixture
Loading pin
Steel Plate for Load Transfer
LVDT
PZT AE Transducer
LVDT
PZT AE Transducer
PZT AE Transducer
PZT AE Transducer
PZT AE Transducer
LVDT
LVDT
Steel Plate for Load Transfer
Adjustable loding block
Loading pin
Loading Fixture
MTS Actuator

Test set-up

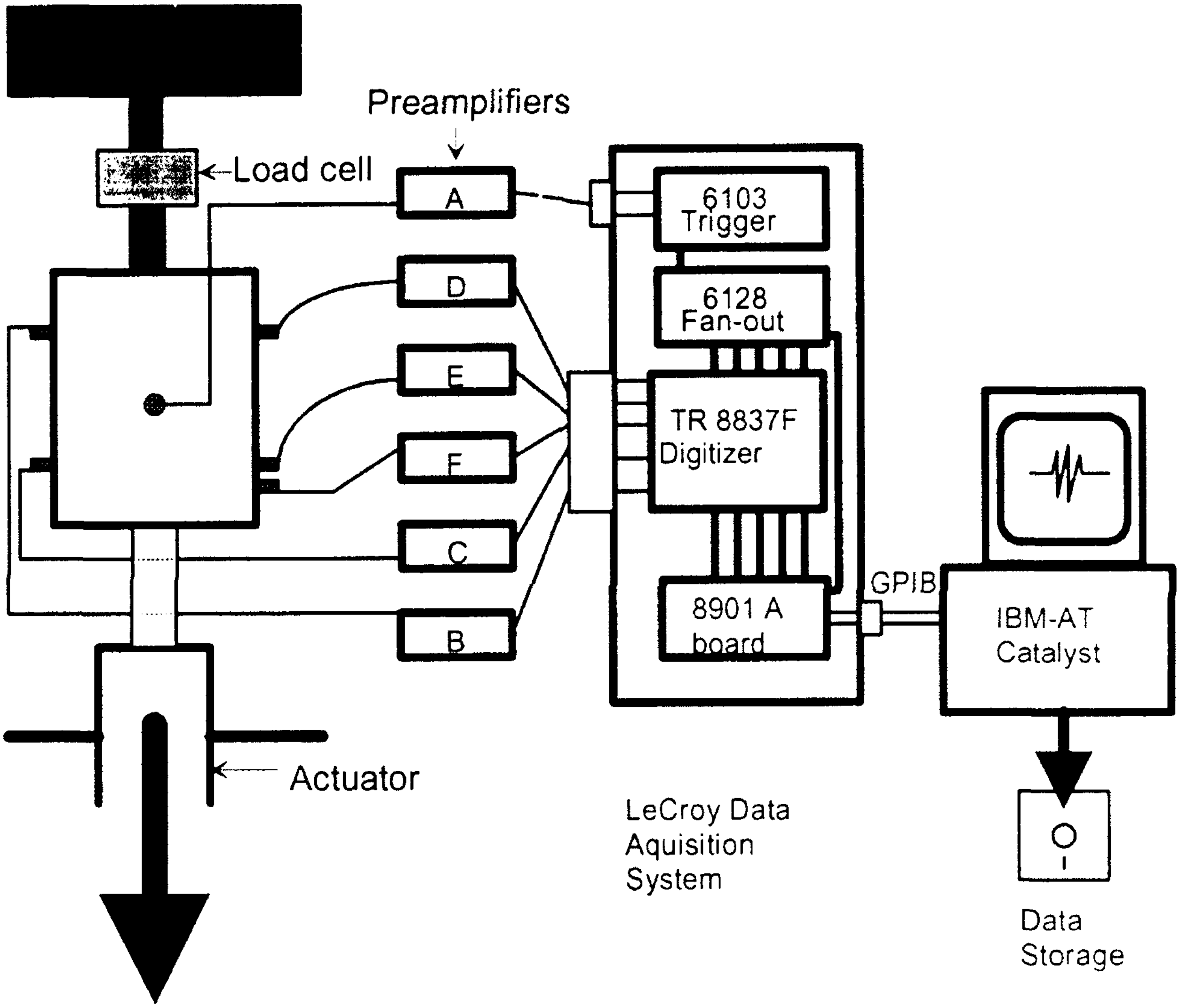

Acoustic emission measurement set up

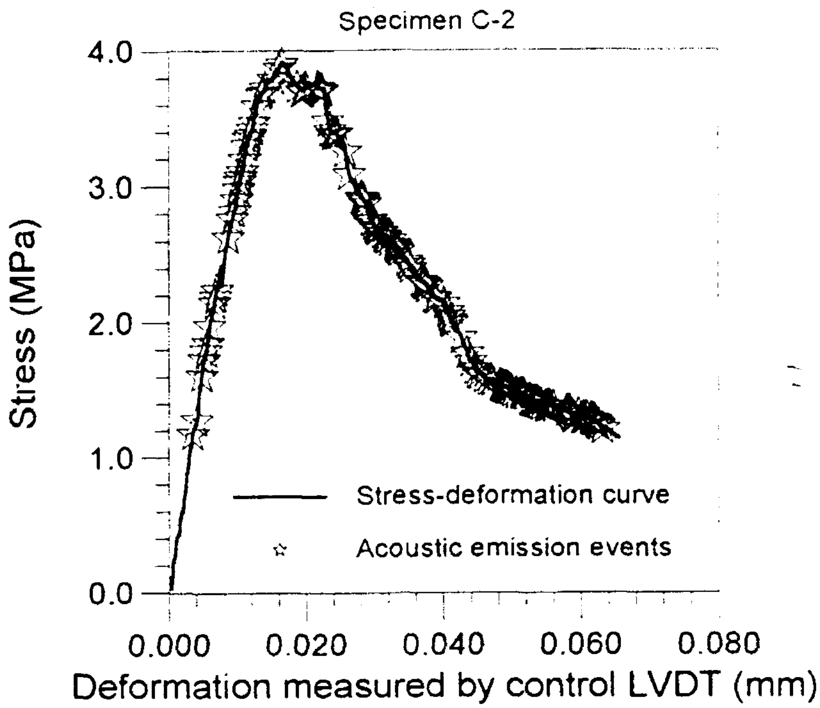
Specimen C-2
4.0
3.0
2.0
1.0
0.0
Stress (MPa)
Stress-deformation curve
Acoustic emission events
0.000
0.020
0.040
0.060
0.080
Deformation measured by control LVDT (mm)

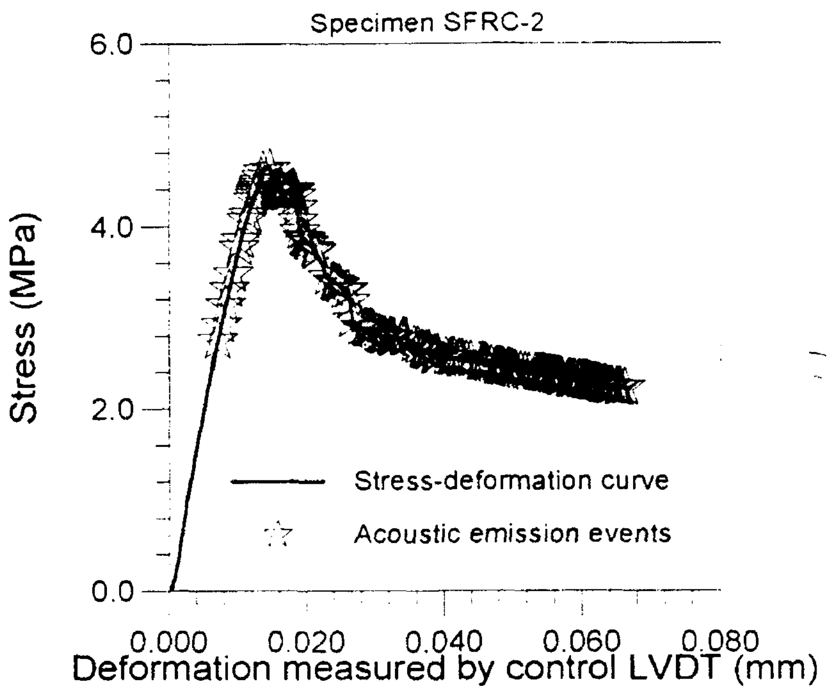
Specimen SFRC-2
6.0
4.0
2.0
0.0
Stress (MPa)
Stress-deformation curve
Acoustic emission events
0.000
0.020
0.040
0.060
0.080
Deformation measured by control LVDT (mm)

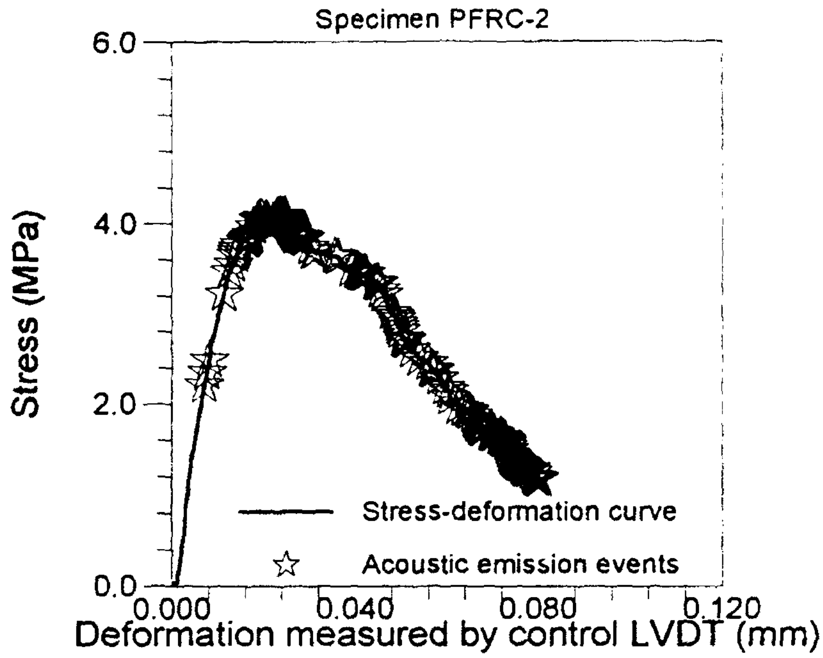
Specimen PFRC-2
6.0
4.0
2.0
0.0
Stress (MPa)
0.000
0.040
0.080
0.120
Deformation measured by control LVDT (mm)
Stress-deformation curve
Acoustic emission events

Fig. 5

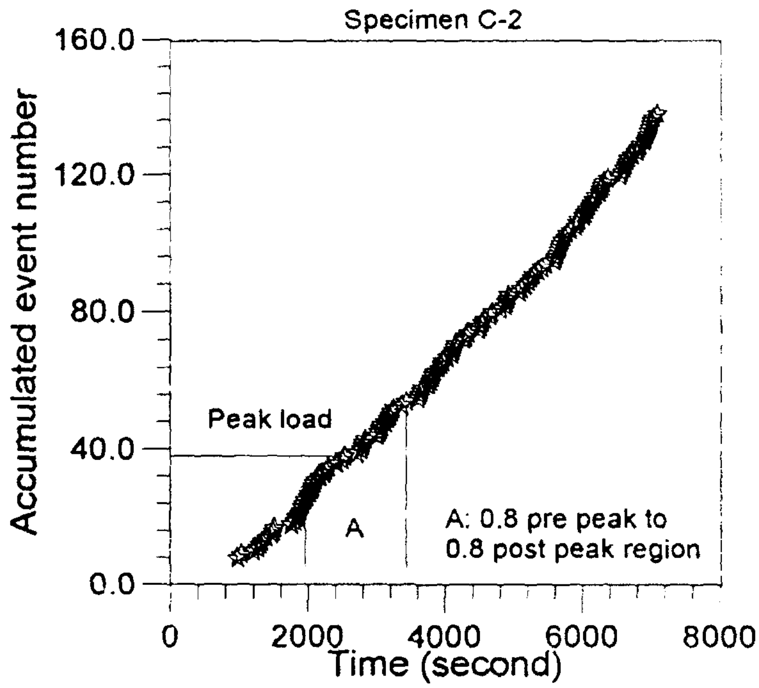
Specimen C-2
160.0
120.0
80.0
40.0
0.0
Accumulated event number
Peak load
A
A: 0.8 pre peak to
0.8 post peak region
0
2000
4000
6000
8000
Time (second)

Fig. 6

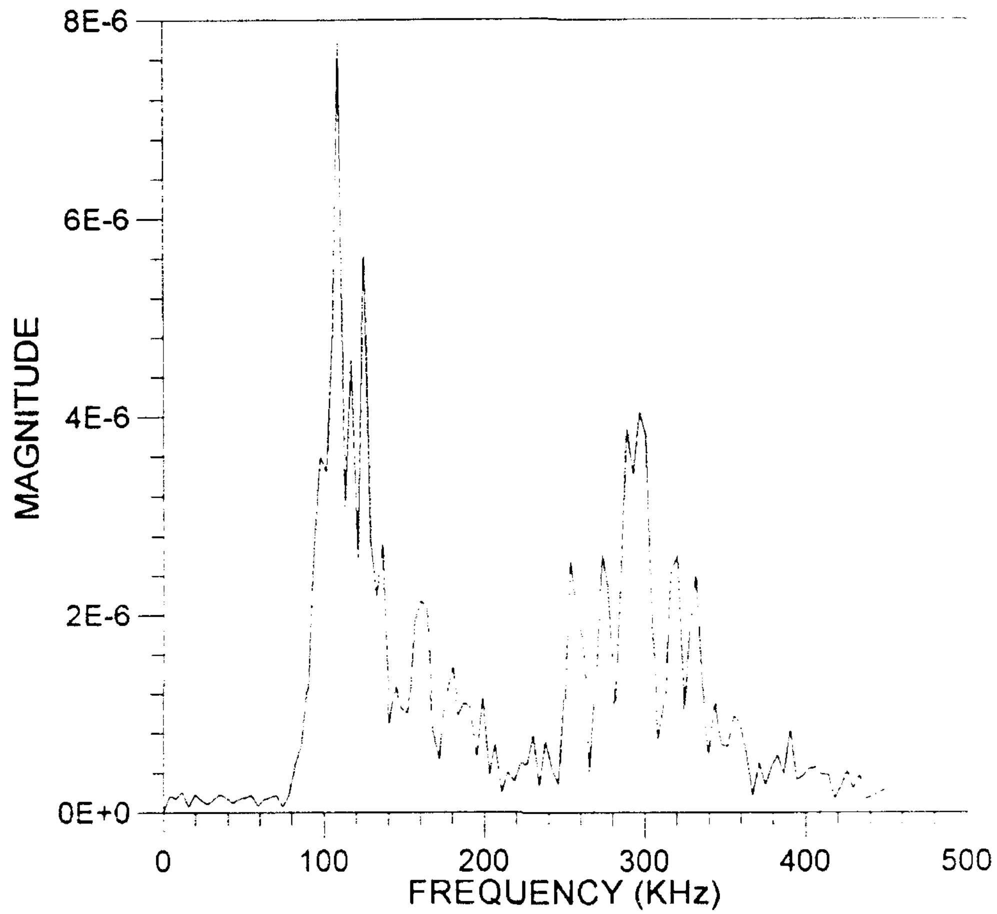
8E-6
6E-6
4E-6
2E-6
0E+0
MAGNITUDE
0
100
200
300
400
500
FREQUENCY (KHz)

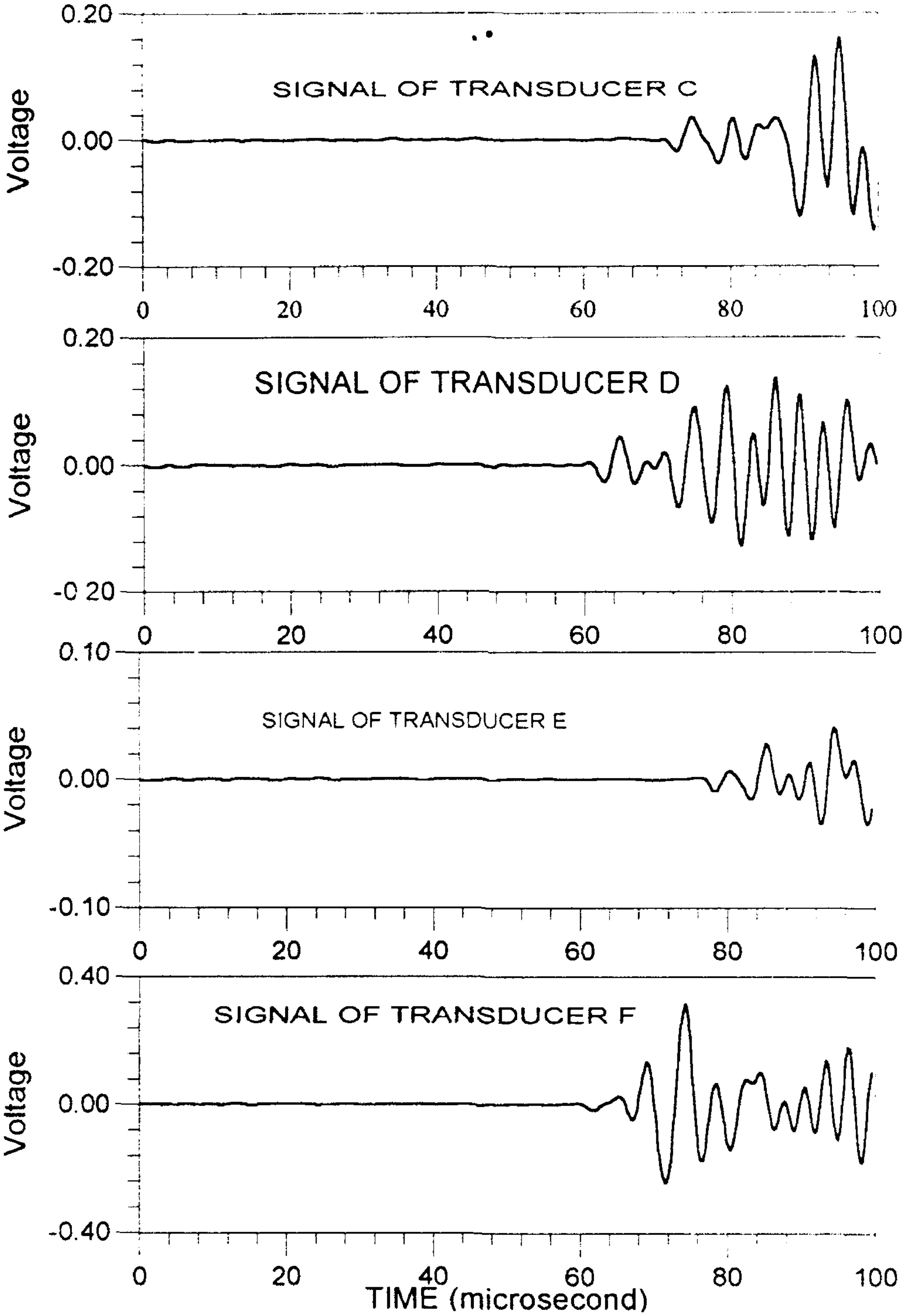
SIGNAL OF TRANSDUCER C
SIGNAL OF TRANSDUCER D
SIGNAL OF TRANSDUCER E
SIGNAL OF TRANSDUCER F
Voltage
0.20
0.00
-0.20
0.10
-0.10
0.40
-0.40
0
20
40
60
80
100
TIME (microsecond)

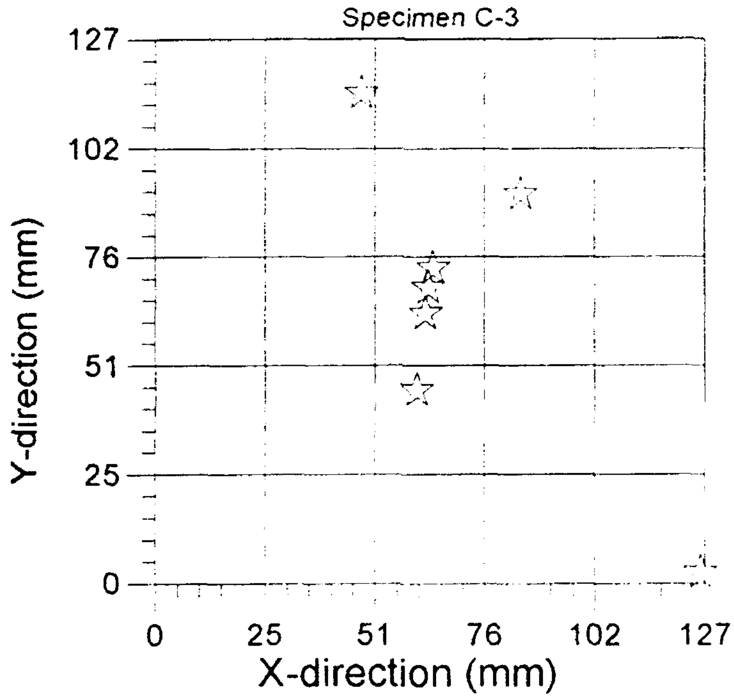

Specimen C-3
127
102
76
51
25
0
Y-direction (mm)
0
25
51
76
102
127
X-direction (mm)

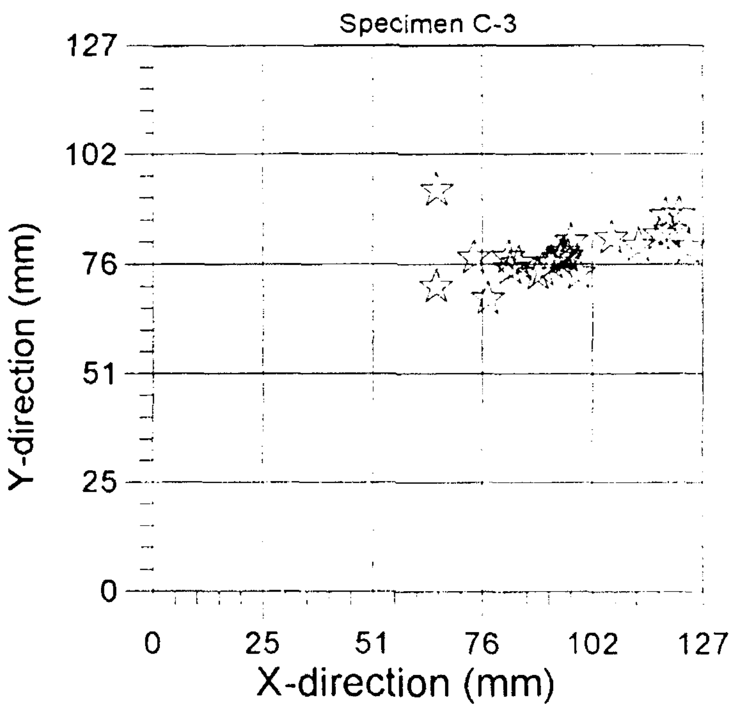

Specimen C-3
127
102
76
51
25
0
Y-direction (mm)
0
25
51
76
102
127
X-direction (mm)

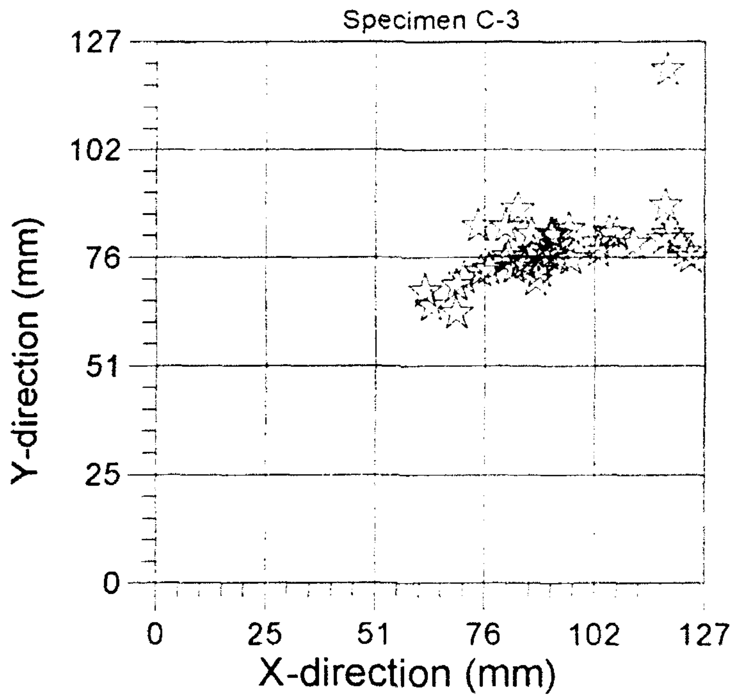
Specimen C-3
127
102
76
51
25
0
0
25
51
76
102
127
Y-direction (mm)
X-direction (mm)

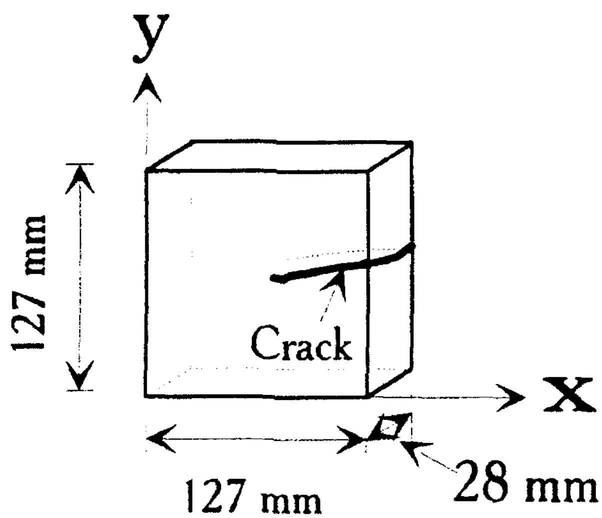
y
x
127 mm
Crack
127 mm
28 mm

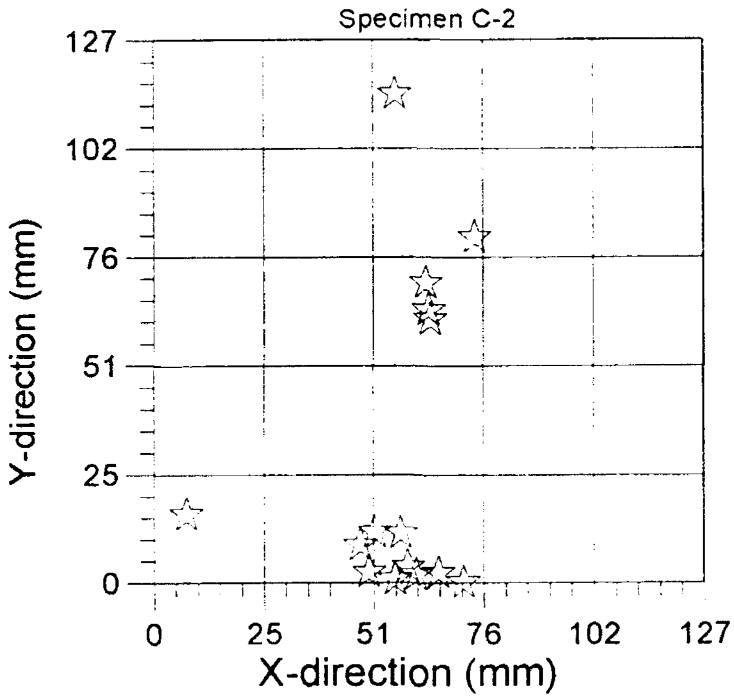
Specimen C-2
127
102
76
51
25
0
0
25
51
76
102
127
Y-direction (mm)
X-direction (mm)

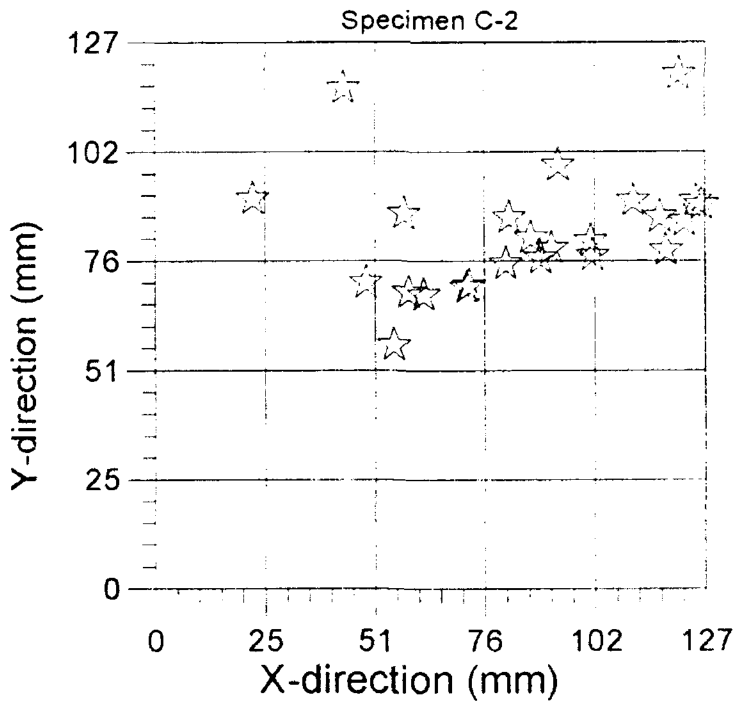
Specimen C-2
127
102
76
51
25
0
0
25
51
76
102
127
Y-direction (mm)
X-direction (mm)

p.

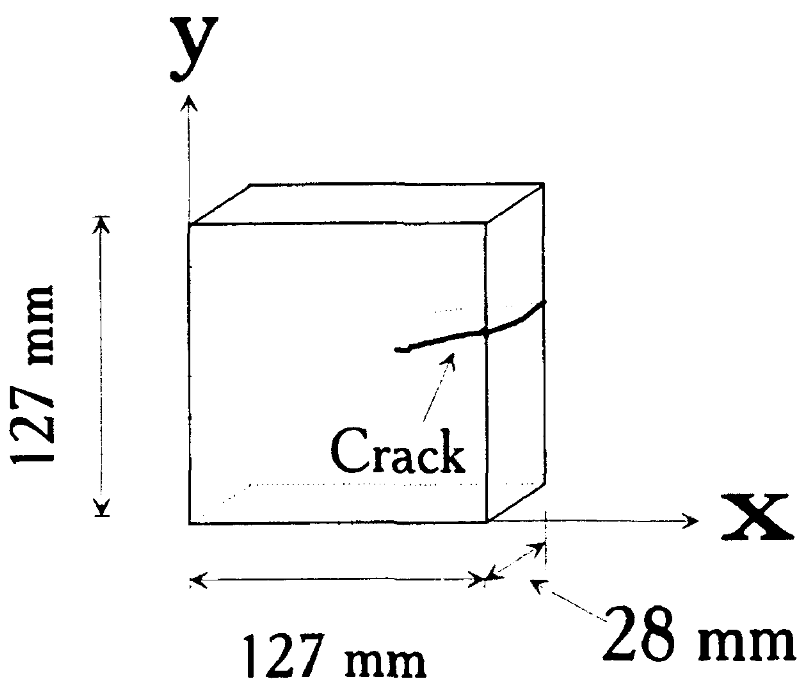

Visible crack position
for concrete specimen
C-2

Fig 12

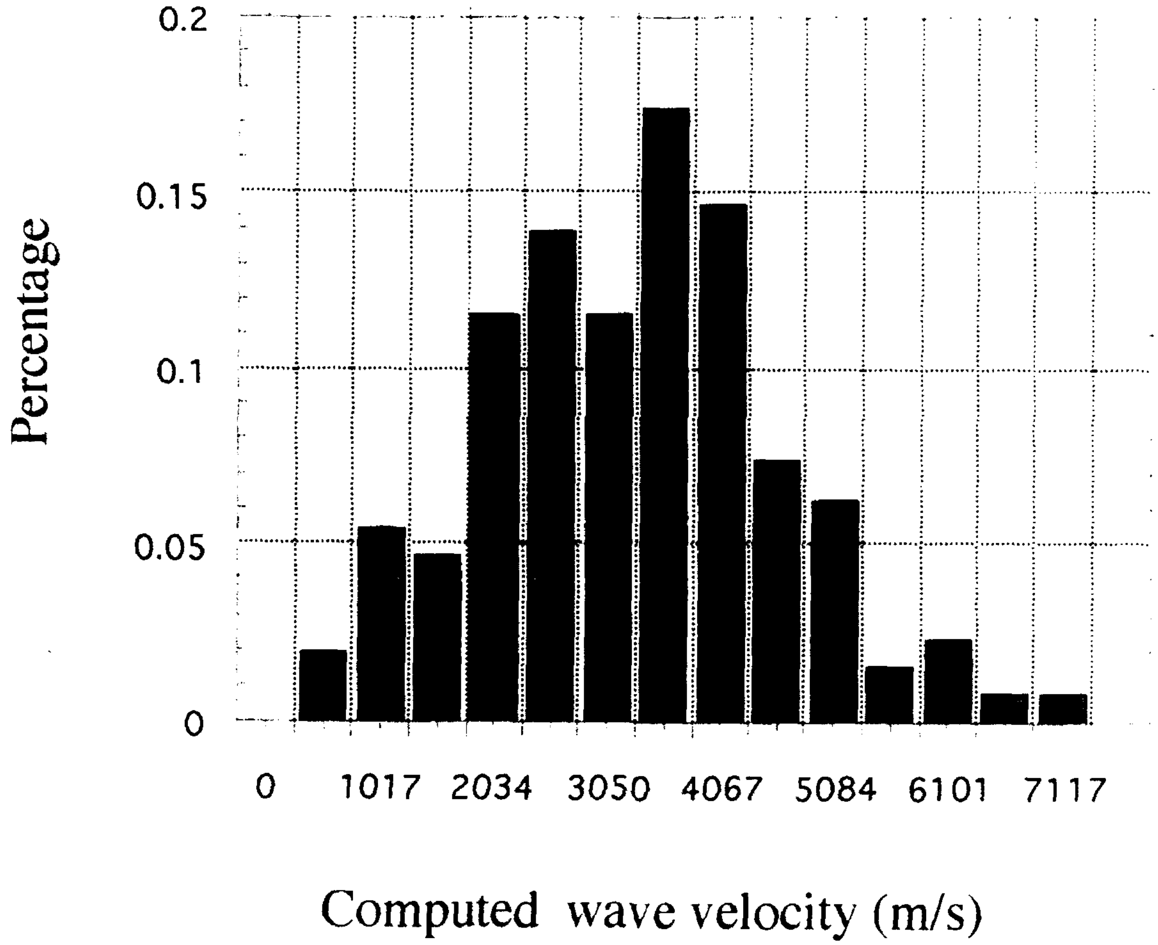
0.2
0.15
0.1
0.05
0
Percentage
0
1017
2034
3050
4067
5084
6101
7117
Computed wave velocity (m/s)

Fig. 13

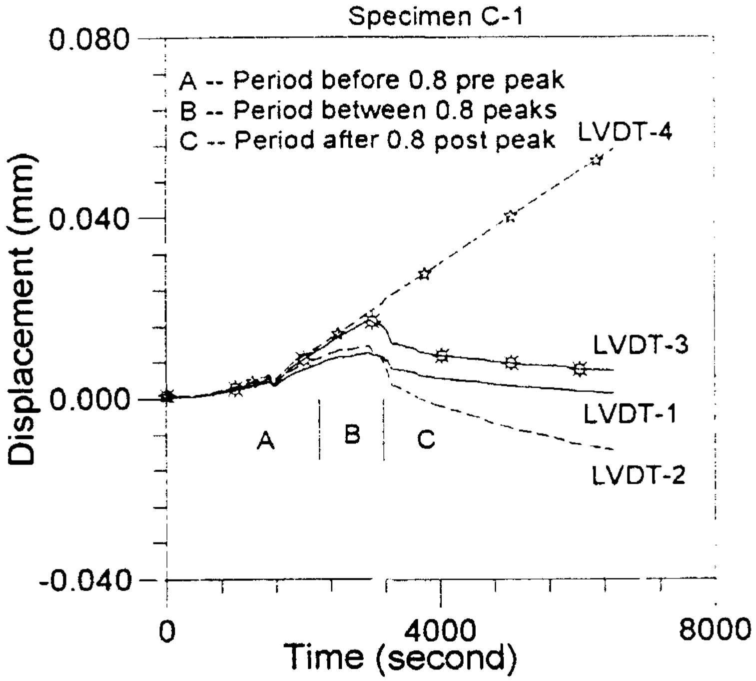
Specimen C-1
A -- Period before 0.8 pre peak
B -- Period between 0.8 peaks
C -- Period after 0.8 post peak
LVDT-4
LVDT-3
LVDT-1
LVDT-2
A
B
C
Displacement (mm)
0.080
0.040
0.000
-0.040
0
4000
8000
Time (second)

Fig. —

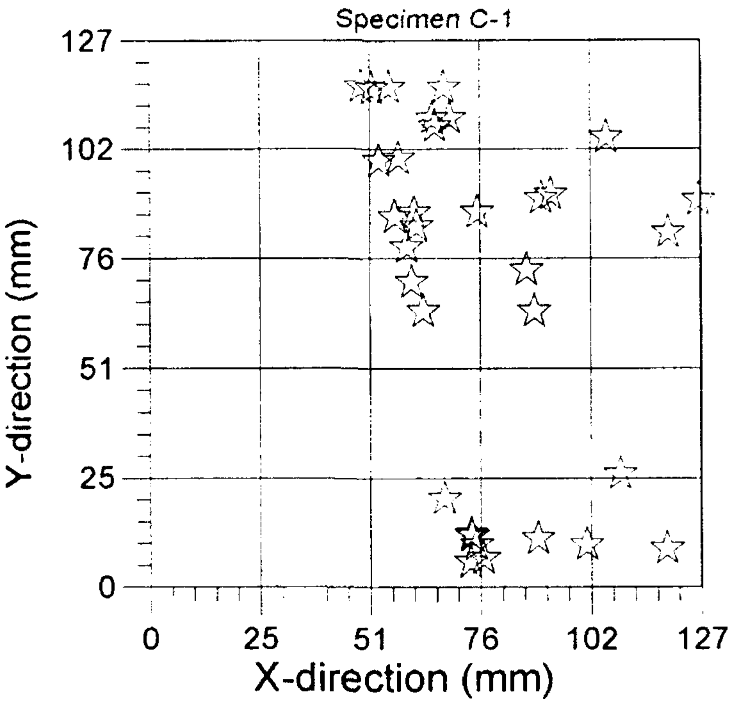
Specimen C-1
127
102
76
51
25
0
Y-direction (mm)
0
25
51
76
102
127
X-direction (mm)

Fig. 5 ..

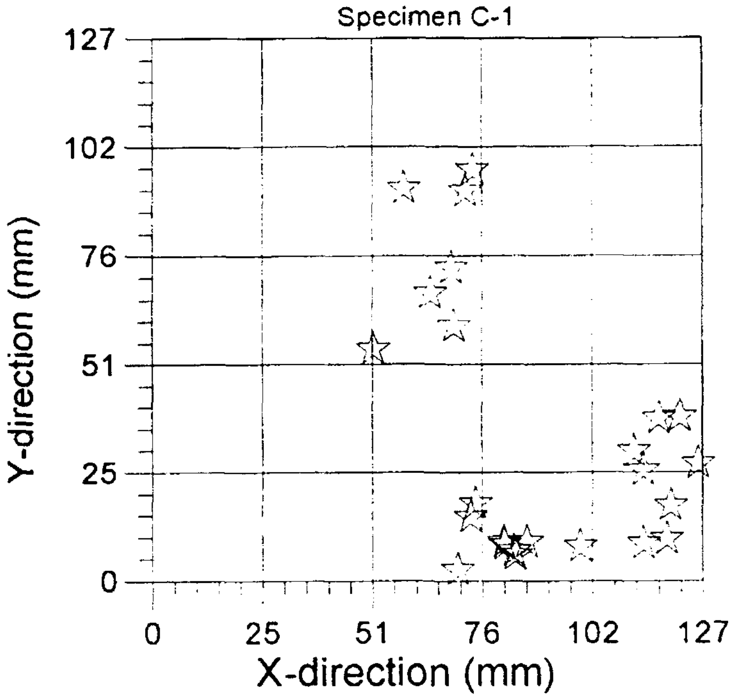
Specimen C-1
127
102
76
51
25
0
0
25
51
76
102
127
X-direction (mm)
Y-direction (mm)

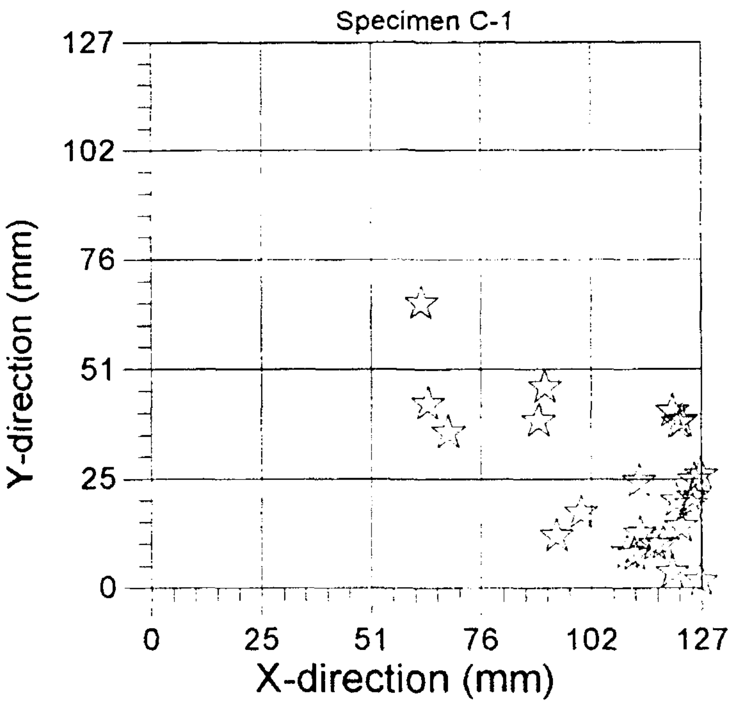
Specimen C-1
127
102
76
51
25
0
0
25
51
76
102
127
X-direction (mm)
Y-direction (mm)

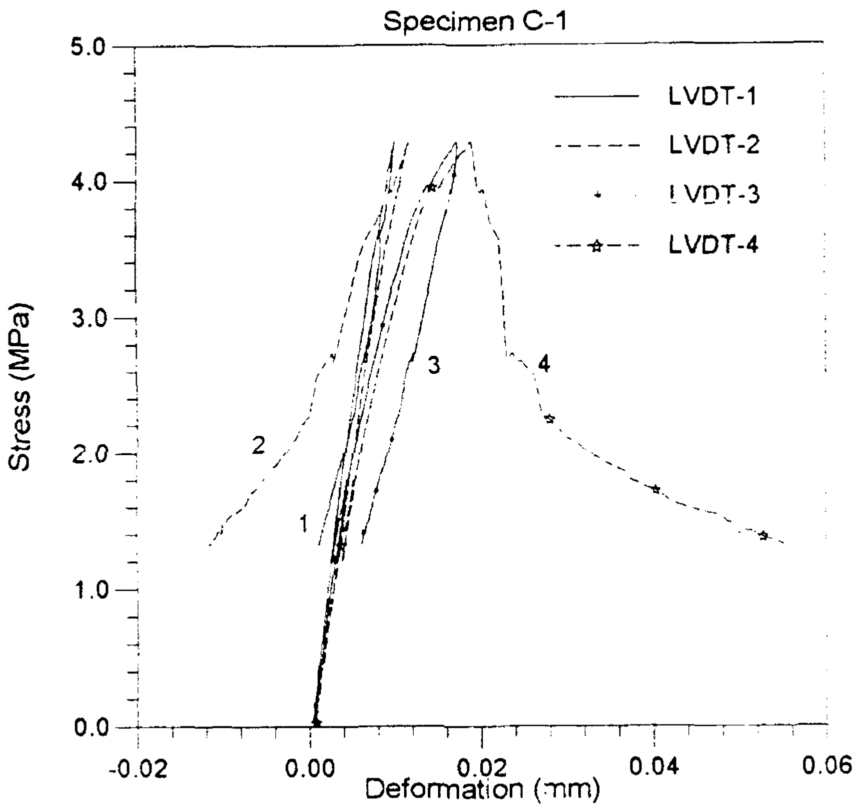
Specimen C-1
Stress (MPa)
Deformation (mm)
LVDT-1
LVDT-2
LVDT-3
LVDT-4
5.0
4.0
3.0
2.0
1.0
0.0
-0.02
0.00
0.02
0.04
0.06
1
2
3
4

Fig. 1